ISSN 2410-3462

Volume 9, Issue 26 – January – June - 2022

Journal Simulation and Laboratory

ECORFAN®

Journal Simulation and Laboratory, Volume 9, Issue 26, January - June 2022, is a journal edited six monthly by ECORFAN-Bolivia. 21 Loa 1179, Cd. Sucre. Chuquisaca, Bolivia. WEB: www.ecorfan.org, revista@ecorfan.org. Chief Editor: SERRANO-PACHECO, Martha. PhD. ISSN-On line: 2410-3462. Responsible for the latest update of this number ECORFAN Computer Unit. ESCAMILLA-BOUCHÁN, Imelda, PhD, LUNA-SOTO, Vladimir. PhD. Loa 1179, Cd. Sucre. Chuquisaca, Bolivia, last updated June 30, 2022.

Journal Simulation and Laboratory

Definition of Research Journal

Scientific Objectives

Support the international scientific community in its written production Science, Technology and Innovation in the Field of Biology and Chemistry, in Subdisciplines of movement, sound and energy, thermoelectricity, quantum phenomena, molecular biology, molecular biology of microorganisms, molecular biology of plants, microbiological chemistry, cellular morphology, general chemistry, quantum chemistry.

ECORFAN-Mexico SC is a Scientific and Technological Company in contribution to the Human Resource training focused on the continuity in the critical analysis of International Research and is attached to CONACYT-RENIECYT number 1702902, its commitment is to disseminate research and contributions of the International Scientific Community, academic institutions, agencies and entities of the public and private sectors and contribute to the linking of researchers who carry out scientific activities, technological developments and training of specialized human resources with governments, companies and social organizations.

Encourage the interlocution of the International Scientific Community with other Study Centers in Mexico and abroad and promote a wide incorporation of academics, specialists and researchers to the publication in Science Structures of Autonomous Universities - State Public Universities - Federal IES - Polytechnic Universities - Technological Universities - Federal Technological Institutes - Normal Schools - Decentralized Technological Institutes - Intercultural Universities - S & T Councils - CONACYT Research Centers.

Scope, Coverage and Audience

Journal Simulation and Laboratory is a Research Journal edited by ECORFAN-Mexico S.C in its Holding with repository in Bolivia, is a scientific publication arbitrated and indexed with semester periods. It supports a wide range of contents that are evaluated by academic peers by the Double-Blind method, around subjects related to the theory and practice of movement, sound and energy, thermoelectricity, quantum phenomena, molecular biology, molecular biology of microorganisms, molecular biology of plants, microbiological chemistry, cellular morphology, general chemistry, quantum chemistry with diverse approaches and perspectives, that contribute to the diffusion of the development of Science Technology and Innovation that allow the arguments related to the decision making and influence in the formulation of international policies in the Field of Biology and Chemistry. The editorial horizon of ECORFAN-Mexico® extends beyond the academy and integrates other segments of research and analysis outside the scope, as long as they meet the requirements of rigorous argumentative and scientific, as well as addressing issues of general and current interest of the International Scientific Society.

Editorial Board

Arbitration Committee

Assignment of Rights

The sending of an Article to Journal Simulation and Laboratory emanates the commitment of the author not to submit it simultaneously to the consideration of other series publications for it must complement the Originality Format for its Article.

The authors sign the Authorization Format for their Article to be disseminated by means that ECORFAN-Mexico, S.C. In its Holding Bolivia considers pertinent for disclosure and diffusion of its Article its Rights of Work.

Declaration of Authorship

Indicate the Name of Author and Coauthors at most in the participation of the Article and indicate in extensive the Institutional Affiliation indicating the Department.

Identify the Name of Author and Coauthors at most with the CVU Scholarship Number-PNPC or SNI-CONACYT- Indicating the Researcher Level and their Google Scholar Profile to verify their Citation Level and H index.

Identify the Name of Author and Coauthors at most in the Science and Technology Profiles widely accepted by the International Scientific Community ORC ID - Researcher ID Thomson - arXiv Author ID - PubMed Author ID - Open ID respectively.

Indicate the contact for correspondence to the Author (Mail and Telephone) and indicate the Researcher who contributes as the first Author of the Article.

Plagiarism Detection

All Articles will be tested by plagiarism software PLAGSCAN if a plagiarism level is detected Positive will not be sent to arbitration and will be rescinded of the reception of the Article notifying the Authors responsible, claiming that academic plagiarism is criminalized in the Penal Code.

Arbitration Process

All Articles will be evaluated by academic peers by the Double Blind method, the Arbitration Approval is a requirement for the Editorial Board to make a final decision that will be final in all cases. MARVID® is a derivative brand of ECORFAN® specialized in providing the expert evaluators all of them with Doctorate degree and distinction of International Researchers in the respective Councils of Science and Technology the counterpart of CONACYT for the chapters of America-Europe-Asia- Africa and Oceania. The identification of the authorship should only appear on a first removable page, in order to ensure that the Arbitration process is anonymous and covers the following stages: Identification of the Research Journal with its author occupation rate - Identification of Authors and Coauthors - Detection of plagiarism PLAGSCAN - Review of Formats of Authorization and Originality-Allocation to the Editorial Board- Allocation of the pair of Expert Arbitrators-Notification of Arbitration -Declaration of observations to the Author-Verification of Article Modified for Editing-Publication.

Instructions for Scientific, Technological and Innovation Publication

Knowledge Area

The works must be unpublished and refer to topics of movement, sound and energy, thermoelectricity, quantum phenomena, molecular biology, molecular biology of microorganisms, molecular biology of plants, microbiological chemistry, cellular morphology, general chemistry, quantum chemistry and other topics related to Biology and Chemistry.

Presentation of the content

In the first article we present, *Storm surge forecast calculus on the Mexican Pacific coast using SWASH numerical model* by AGUILERA-MENDEZ, José María, JUAREZ-TOLEDO, Carlos, CALDERON-MAYA, Juan Roberto and MARTINEZ-CARRILLO, Irma, with adscription in the Universidad Autónoma del Estado de México, in the next article we present, *Preparation of catalytic materials for obtaining Acrylic Acid from Ethylene and Carbon Dioxide* by CANUL-CEMÉ, Carina Ivonne, CONEJO-FLORES, Ricardo, GARCÍA-GONZÁLEZ, Juan Manuel and GUZMÁN-PANTOJA, Javier, with adscription in the Universidad Autónoma de Zacatecas and Gerencia de Refinación de Hidrocarburos, Instituto Mexicano del Petróleo, in the next article we present, *Simulation of gas condensation process from pyrolysis of used tires* by MORENO-ARIAS, Claudio Alberto, CHAMARRAVÍ-GUERRA, Oscar and LOPÉZ-MAZA, Fernando de Jesús, with adscription in the Fundación Universidad de América, in the last article we present, *Temperature Profile Estimation in the Core of a Sodium-Cooled Fast Reactor using CFD Modeling* by DIAZ-ESPINOZA, Gerardo, VALLE-HERNANDEZ, Julio and GALLARDO-VILLARREAL, José Manuel, with adscription in the Universidad Politécnica Metropolitana de Hidalgo and Universidad Autónoma del Estado de Hidalgo.

Content

Article **Journal Simulation and Laboratory**
June 2022 Vol.9 No.26 1-8

Storm surge forecast calculus on the Mexican Pacific coast using SWASH numerical model

Cálculo del pronóstico de marea de tormenta en la costa del pacífico mexicano utilizando el modelo numérico SWASH

AGUILERA-MENDEZ, José María†*, JUAREZ-TOLEDO, Carlos, CALDERON-MAYA, Juan Roberto and MARTINEZ-CARRILLO, Irma

Universidad Autónoma del Estado de México, Unidad Académica Profesional Tianguistenco.

ID 1st Author: *José María, Aguilera-Méndez* / **ORC ID**: 0000-0002-9826-421X, **CVU CONACYT ID**: 66670

ID 1st Co-author: *Carlos, Juárez-Toledo* / **ORC ID**: 0000-0002-7440-3246, **Researcher ID Thomson**: C-1368-2016, **CVU CONACYT ID**: 39912

ID 2nd Co-author: *Juan Roberto, Calderón-Maya* / **ORC ID**: 0000-0002-6584-8868, **Researcher ID Thomson**: B-1604-2016, **CVU CONACYT ID**: 100490

ID 3rd Co-author: *Irma, Martínez-Carrillo* / **ORC ID**: 0000-0002-7952-4418, **Researcher ID Thomson**: B-9264-2016, **CVU CONACYT ID**: 39914

DOI: 10.35429/JSL.2022.26.9.1.8 Received March 30 2022; Accepted June 30, 2022

Abstract

Storm surge is a phenomenon that occurs on coasts with a higher incidence in the rainy season. The factors that promote its appearance are the wind and the tide whose force has been sometimes catastrophic. The objective of the study is to provide a storm surge forecast using the SWASH numerical model for some points on the Mexican Pacific coast. The approach of the experiment refers to previous works that use the infrastructure and data available from NOAA and SEMAR; the use of unstructured meshes used in a wave model to conclude in a beach wave model. In the validation of the results, the tide gauges of the study locations will be used; with the feedback obtained, the necessary adjustments are expected until the model has at least 60% correct measurements. Some authors agree that global warming affects the power with which the phenomenon has been manifesting itself, so that the development of technology could help minimize the consequences.

Storm surge, SWASH model, Unstructured mesh

Resumen

La marea de tormenta es un fenómeno que se presenta en costas con una mayor incidencia en temporada de lluvias. Los factores que promueven su aparición son el viento y la marea cuya fuerza ha resultado en ocasiones catastrófica. El objetivo del estudio es proveer un pronóstico de marea de tormenta usando el modelo numérico SWASH para algunos puntos de la costa del pacífico mexicano. El planteamiento del experimento hace referencia de trabajos anteriores que utilizan la infraestructura y datos disponibles de la NOAA y SEMAR; el uso de mallas no estructuradas utilizadas en un modelo de oleaje para concluir en un modelo de olas de playa. En la validación de los resultados se utilizarán los mareógrafos de las localidades de estudio; con la retroalimentación obtenida, se esperan los ajustes necesarios hasta que el modelo tenga al menos 60% de mediciones acertadas. Algunos autores concuerdan con que el calentamiento global incide en la potencia con la que el fenómeno se ha venido manifestando, por lo que el desarrollo de la tecnología pudiera ayudar a minimizar las consecuencias.

Ola de tormenta, Modelo SWASH, Malla no estructurada

Citation: AGUILERA-MENDEZ, José María, JUAREZ-TOLEDO, Carlos, CALDERON-MAYA, Juan Roberto and MARTINEZ-CARRILLO, Irma. Storm surge forecast calculus on the Mexican Pacific coast using SWASH numerical model. Journal Simulation and Laboratory. 2022, 9-26: 1-8

*Correspondence to Author (e-mail: jaguileram001@alumno.uaemex.mx)
†Researcher contributing as first Author.

Introduction

This article describes the first stage of the project that seeks to implement a storm surge forecasting model along the Mexican coast. The paper explains the SWASH numerical model (Delft University of Technology (TUDelft), n.d.) implementation as an accurate low cost open source alternative for storm surge forecasting. The storm surge phenomenon is described by the world meteorological organization as "an abnormal rise of water generated by a storm. Strong winds in a tropical cyclone or a sever mid-latitude storm are their primary cause.

However, ocean bottom topography, tides, waves and freshwater input from rivers affect the water level rise during a storm surge. The depth of a storm surge can rise quickly — from centimeters to a meter or more in a matter of minutes. It can push an incredible distance beyond the coast.". (Bautista *et al*., 2001; World Meteorological Organization (WMO), n.d.) Once the components of the phenomenon have been described, its magnitude is understood until the affectations derived from its formation are evaluated; for example during Hurricane Ike, the storm surge reached up to 50 kilometers inland (Musinguzi *et a*l., 2019). A storm surge can travel across bays and up rivers, in essence, it can traverse any body of water that is on or near the shoreline as showed in Figure 1.

Carrying out a couple of calculations, one cubic meter of seawater (at 20 °C) weighs 1,024 kilos, that is, just over a ton. Thus, a storm surge carrying tons of water at speeds typically between 15 and 25 kilometers per hour has enormous force. A 50-centimeter storm surge can easily carry a car away, and it would be difficult for an adult to stand up against a 15-centimeter storm surge.

It is necessary to remember that by definition, the forecasts wave heights are the Significant Wave Height (Hsig); this is the average wave height (trough to crest) of the highest 1/3 of the forecast waves (Aguilera-Méndez *et al*., 2022; Luke, 2006; Pecher & Kofoed, 2017; Zijlema, 2010). This definition is valid for waves generated in a storm surge forecast, that is, the prediction generated for storm surge also indicate that proportion of the wave; so its interpretation must consider the theory that supports these developments.

As a consequence of this measurement, we will continue using the *seas* variable (Aguilera-Méndez *et al*., 2022) in the calculations of the experiment.

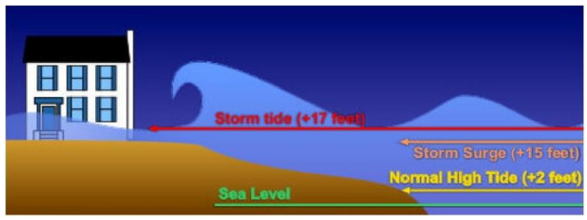

Figure 1 Storm surge
Source NOAA https://www.aoml.noaa.gov/es/hrd-faq/#storm-surge-v-tide

The formulas to generate the storm surge simulation are based on wave equations. The elevation of the water surface ζ is given by Equation 1:

$$\zeta = \frac{H}{2} cos\left[2\pi\left(\frac{x}{\lambda} - \frac{t}{T}\right)\right] \quad (1)$$

The change in ocean surface elevation is the result of an elliptical motion of water particles, which extends below the surface. This movement is mainly affected by the wind speed and direction as well as the amount of water below the wave and the bathymetry (Aguilera-Méndez, Juárez-Toledo, Martínez-Carrillo, & Vera-Popoca, 2021; Pecher & Kofoed, 2017). As the changes in the storm surge are very fast, the equations used change considerably to establish a more realistic pattern, as shown by the equations used in Rijnsdorp's work (Rijnsdorp & Zijlema, 2016) where they propose the Equations 2, 3 and 4.

$$\frac{\partial u}{\partial x} + \frac{\partial w}{\partial z} = 0, \quad (2)$$

$$\frac{\partial u}{\partial t} + \frac{\partial uu}{\partial x} + \frac{\partial wu}{\partial z} = -g\frac{\partial \zeta}{\partial x} - \frac{\partial p}{\partial x} + \frac{\partial \tau_{xx}}{\partial x} + \frac{\partial \tau_{xz}}{\partial z}, \quad (3)$$

$$\frac{\partial w}{\partial t} + \frac{\partial uw}{\partial x} + \frac{\partial ww}{\partial z} = -\frac{\partial p}{\partial z} + \frac{\partial \tau_{zx}}{\partial x} + \frac{\partial \tau_{zz}}{\partial z} \quad (4)$$

Where $u(x,z,t)$ is the velocity in x direction, $w(x,z,t)$ is the velocity in z direction, g is the gravitational acceleration, $\tau\,(x,z,t)$ represents the turbulent stresses, $p(x,z,t)$ is the non-hydrostatic pressure (normalized by a reference density), and $\zeta(x,t)$ is the piezometric head (which is equivalent to the free surface in the outer domain).

ISSN: 2410-3462

From Equation 2 which is the simple way to represent the hydrodynamic flow or wave movement on beaches they includes the gravitational factor and third axe to represent the internal wave movement in Equation 3; making a factor reduction and substitution they get Equation 4, which is the simplest way of wave movement in the SWASH numerical model.

In order to be functional, numerical storm surge forecast models must be applied in relatively small areas if their information is to be as close to reality as possible. As the interest of the forecaster is to know the places where the waves could impact with greater force, the information that is generated must be precise (Mcinnes *et al*., 2003; Musinguzi *et al*., 2019), leaving the global behavior of the tides and waves to the macro models. In this stage of the project, the calculation of storm surge was implemented in places where meteorological stations are located and with this, have reference and comparison measurements.

The meteorological stations with which we worked recorded the information every 60 seconds. Therefore, it will be taken as a measure for the simple comparison of the results; as well as in a second analysis using the mean square error method. The criterion to consider the resulting model as successful will be that the predicted data is within a range greater than or equal to 60% of approximation; even considering the Hsig criterion.

One aspect to keep in mind is the processing capacity available. Any model that grows in complexity necessarily reflects it in the time it takes to run the simulations and in their memory and disk space requirements. The computer where the operational model is mounted has 12 Pentium7 cores at 3.0 MHz, 128 GB memory, 500 GB storage on SSD and was compiled using gcc and gfortran on 64-bit Linux with MPICH libraries. Both SWAN and SWASH models were compiled using the parallel processing option; the product that is expected from the simulation of the 20 defined points, showed on Table 1, is an 8-hour forecast on the behavior of the waves on the beach. Simulation run time is expected to be 60 minutes.

Puerto Chiapas	Huatulco	Puerto Escondido	Salina Cruz
Puerto Vallarta	Isla Roqueta	Isla María Madre	Lázaro Cárdenas
Tuxtla	Manzanillo	Acapulco	San Blas
Zihuatanejo	San Lucas	Mazatlán	Los Cabos
La Paz	Guaymas	Ensenada	Rosarito

Table 1 Piers with weather stations that were considered in the study
Own Elaboration

Development

The locations that were modelled are indicated in Figure 2. Only those belonging to the Pacific Ocean coast; those found in the Atlantic Ocean will be the subject of further study, mainly due to the difference in sea physical conditions.

The development of the project was carried out using the procedure described by Aguilera (Aguilera-Méndez *et al*., 2022) where the Delaunay diagram is generated for each location, bathymetry data is obtained from the GEBCO site (GEBCO Compilation Group, 2021), data on waves and wind are downloaded from NOAA (*Global Forecast System*, n.d.; *WaveWatch III (WW3) Global Wave Model*, 2019). Once the information had been gathered and the SWAN model (Deftl University of Technology (TUDeftl), n.d.) had fulfilled the parameters, the model was executed. The marine physics variables were considered with the default model values, as well as the GEN3 calculations offered by SWAN and the RIPPLES quotient was used for friction. The regions into which the coastal strip was divided are identified in Figure 3.

Figure 2 Location of weather stations; dots in black mark those selected for the study Mexican Navy
https://meteorologia.semar.gob.mx/

ISSN: 2410-3462

One characteristic that the results of the SWAN numerical model can provide is the tabulation of different variables for a specific coordinate, with the understanding that it is within the defined domain; Thus, in order to obtain the value of the different variables that the SWASH numerical model needs for the execution of our study, the different coordinates of the points on the beach that are closest to the meteorological stations were declared.

The basis of the experiments was the model proposed by the developers for the case: Wind setup in closed basin, test 1: absolute wind velocity. Therefore the variables requested from the SWAN were sea height, wind direction as a vector, wave height and direction. The variables that the SWAN cannot process were captured manually in each definition for the different locations. The objective was to generate an 8 hours simulation for each of the proposed points with the initial conditions indicated by the SWAN using 12:00 (Z) as the start time. Once the model recognized and accepted the values of the variables and the study area was also validated with its bathymetry and the points of the structured mesh; SWASH model execution started processing the requested coordinates as sown in Figure 4.

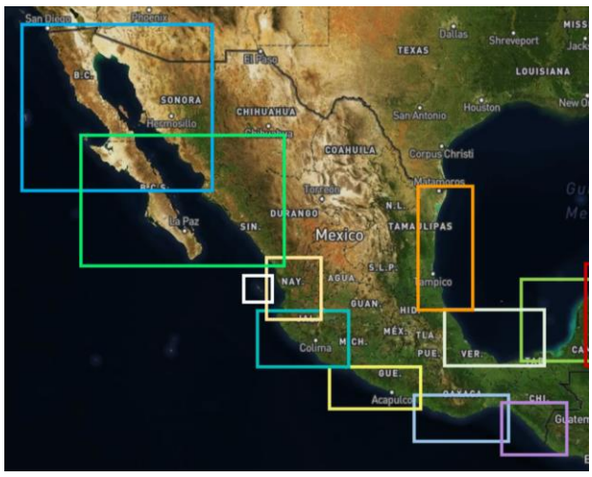

Figure 3 Coastal regions of the Pacific Ocean on which the simulations are carried out. Mexican Navy *https://meteorologia.semar.gob.mx/SWAN/regionSWAN.html*

The SWASH model physics parameters were changed to the same SWAN model physics parameters. To have a consistent principle; so as far as parameterization was possible, the rest of the variables were kept the default value. The most observed variables were those related to the friction and density of the water, because a low-level water coasts and chemistry contamination.

SWASH results were compared against data recorded at weather stations and tide gauges. At this point in the experiment, both the data processed by the model and the observed data were from past events, regardless of the season of the year; the only condition is that the records have a continuity of at least 12 hours, since the simulation configuration contemplates an 8-hour horizon in 60-second intervals given the continuity of the marine flow.

Results

The SWASH model was configured so that the simulation results were saved in a tabular format file; the information was graphed for a better understanding using Matlab. When analyzing the graphs, something that caught our attention was the tendency of the SWASH numerical model to normalize the event after a few hours of simulation. This could be due to the fact that the simulation does not admit more data at the time of execution and consequently, it assumes that there are no more elements that affect its behavior and tends to normalize its movement; doing so, what in natural conditions, the water would tend to stabilize its surface. Figures 5, 6 and 7 show the behavior of the wave simulated by the numerical model. It can be seen that around hour 4 the graph tends to normalize or be harmonic.

```
------------------------------------------------------------
                COMPUTATIONAL PART OF SWASH
------------------------------------------------------------

 One-dimensional mode of SWASH is activated
 Depth-averaged mode of SWASH is activated
 The Cartesian convention for velocity direction is used
 Cartesian coordinate system is used
 Computational grid is rectilinear
 Gridresolution       : MXC            102 MYC              2
                      : MCGRD          103
 Mesh sizes           : DX       0.1000E+03 DY      0.0000E+00
 Drying/flooding      : DEPMIN   0.5000E-04 DPSOPT          2
 Physical constants   : GRAV     0.9813E+01 RHOW    0.1022E+04
                      : RHOA     0.1225E+01 DYNVIS  0.1000E-02
 Wind input           : WSPEED   0.2450E+01 DIR    -0.2570E+01
 Constant wind stress : CD       0.4300E-02
 Chezy formulation    : CF       0.6000E+02
 Vegetation is off
 No wave breaking control
 Baroclinic forcing is off
 No transport of constituent
 Const horz viscosity : VISC     0.0000E+00
 Vertical viscosity is off
 Porosity is off
 Leap-frog scheme     : CFLLOW   0.4000E+00 CFLHIG   0.8000E+00
 Horz advection u-mom : PROPSC          6 KAPPA    0.0000E+00
                      : M        0.2000E+01 PHI     0.0000E+00
 Correction water dep : PROPSC          1 KAPPA    0.0000E+00
                      : M        0.0000E+00 PHI     0.0000E+00
 Sponge layer widths  : LEFT     0.0000E+00 RIGHT   0.0000E+00
                      : LOWER    0.0000E+00 UPPER   0.0000E+00
```

Figure 4 SWASH processing log header
Own Elaboration

ISSN: 2410-3462

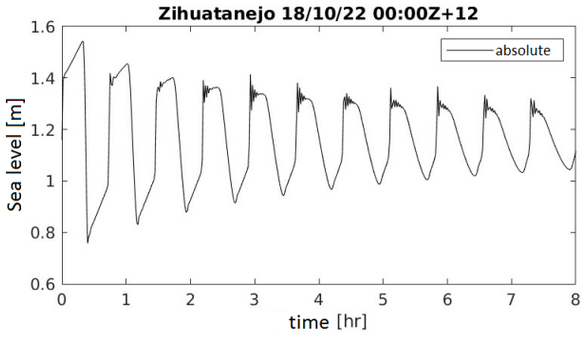

Figure 5 Tidal forecast for Zihuatanejo pier
Own Elaboration

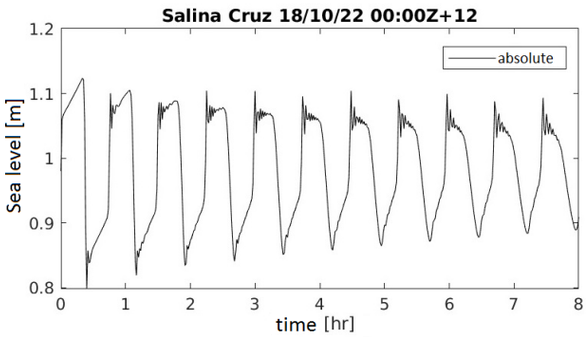

Figure 6 Tidal forecast for Salina Cruz pier
Own Elaboration

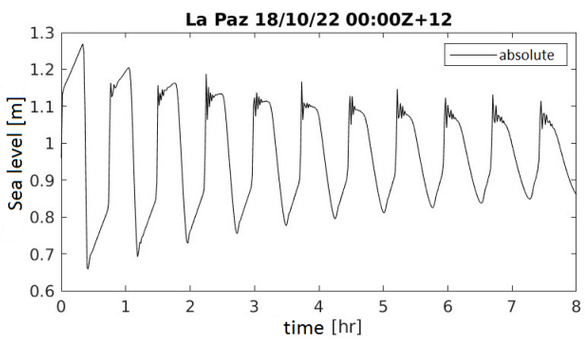

Figure 7 Tidal forecast for La Paz pier
Own Elaboration

After the elaboration of the graphs and the first analysis of the results, the reduction of the simulation time was raised, going from 8 to 3 hours. This change was sought due to two factors: the first has to do with the normalization of wave behavior and its application in highly changing conditions such as the ocean tide and second, the availability of information from different sources; NOAA updates its information in 6-hour periods with 120-hour forecasts; The Meteorological page of Secretary of the Navy (SEMAR, 2019) updates its models every 12 hours with 72-hour forecasts; the configuration of the outputs of the numerical model allow the data to be saved in seconds; For research purposes, the output will be sought every minute for two periods: 1 and 3 hours.

Therefore, there would be information to make the comparisons for one hour or up to three hours in one-minute intervals, so the simulation data would be analyzed prior to the normalization of the wave trend.

With the reduction of the simulation time the processing time was also reduced. Tweaks to the model build also brought better processor performance. With both adjustments it was reduced from an average processing time of 70 to 23 minutes for all domains. The Figure 8, 9 and 10 shows the new data set to be analyzed.

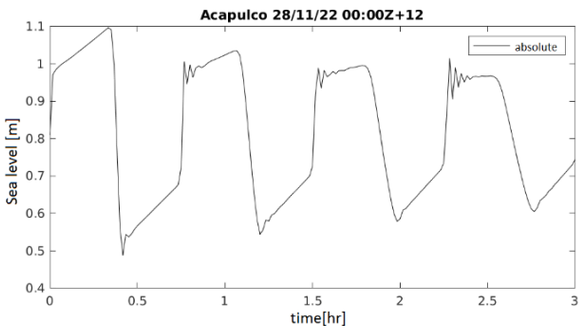

Figure 8 Tidal forecast for Acapulco pier
Own Elaboration

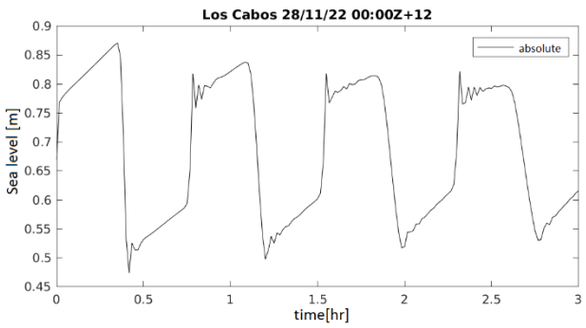

Figure 9 Tidal forecast for Los Cabos pier
Own Elaboration

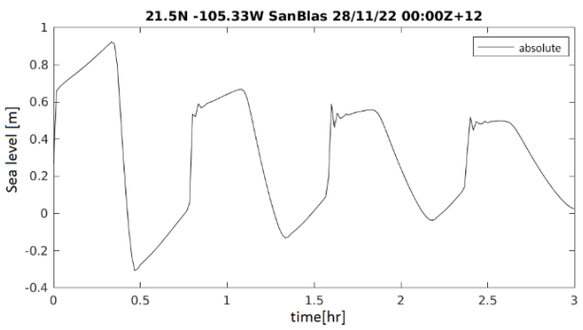

Figure 10 Tidal forecast for San Blas pier
Own Elaboration

ISSN: 2410-3462

This data set was more manageable and allowed a better understanding of wave behavior. It should be noted that the objective of the numerical model is to indicate storm surge height and the probability that it will occur within a time range that in our case is one hour; not so the exact moment in which it could appear.

The graphs generated by the tide gauges were obtained from the captured data. The points comparison was made considering that the information captured from the tide gauges and generated by the numerical model in periods of 1 minute was available. The tide gauges constantly capture information, recording the information every 60 seconds. Depending on the vendor of the equipment and the customer's preferences, these equipment record the average of the height that occurred in the 60 seconds, the weighted average or the result of applying a Fourier transform.

To facilitate the analysis, both graphs are presented instead of data tables. The correspondence of the figures is in pairs; therefore, Figures 11 and 12 correspond to the same point of analysis and so on for the pairs of Figures 13-14 and 15-16.

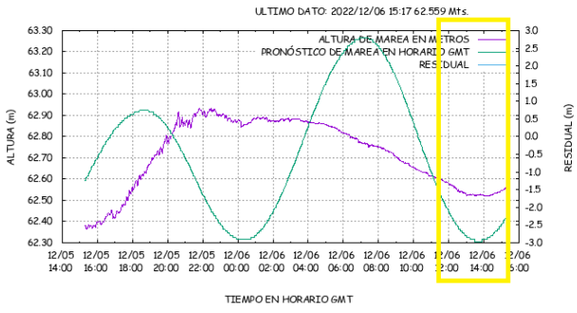

Figure 11 Tide recorded (in red) by the tide gauge located in La Paz pier
Network tide stations. https://oceanografia.semar.gob.mx/mapa_estaciones.html

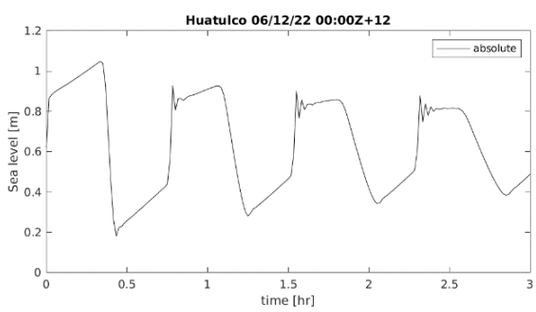

Figure 12 Tidal forecast for Huatulco pier
Own Elaboration

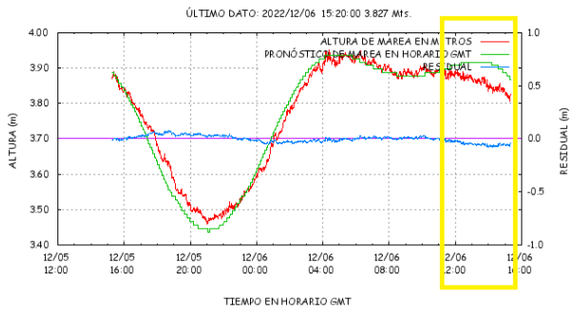

Figure 13 Tide recorded (in red) by the tide gauge located in Lazaro Cárdenas pier
Network tide stations. https://oceanografia.semar.gob.mx/mapa_estaciones.html

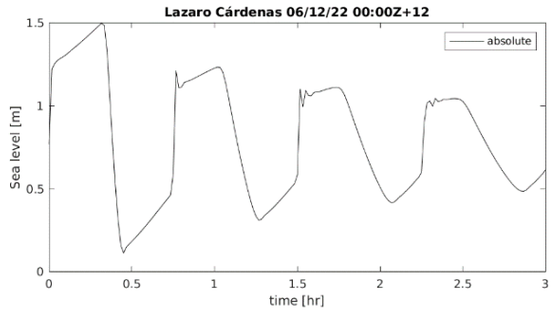

Figure 14 Tidal forecast for Lazaro Cárdenas pier
Network tide stations. https://oceanografia.semar.gob.mx/mapa_estaciones.html

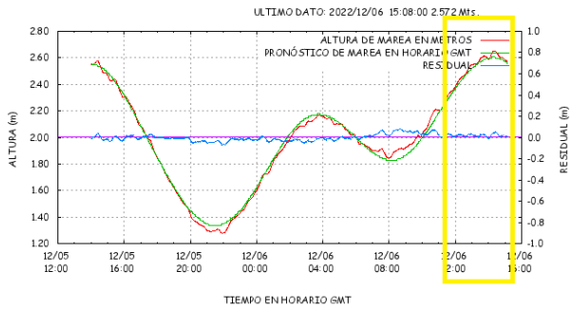

Figure 15 Tide gauge record (in red) for La Paz location
Own Elaboration

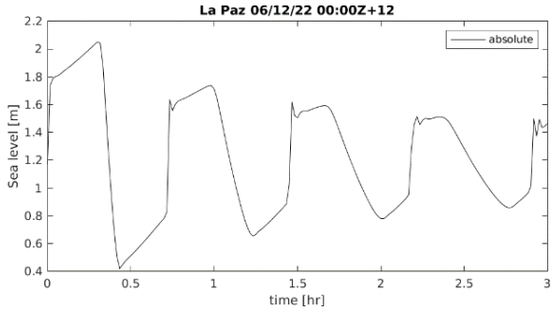

Figure 16 Tidal forecast for La Paz pier
Own Elaboration

ISSN: 2410-3462

Conclusions

The point-to-point analysis of the records showed important discrepancies, so it was discarded as validation. It was replaced by a trend analysis where the results showed a similar behavior within the established range of 60%. Considering that the time and the way in which the record is kept also influences the presentation of the results, it is the analysis of trends over longer periods of time, which will help to better understand the records obtained from the equipment. For this reason, we will work on the data from the tide gauges and the simulation in periods of 48 hours. In the case of the model that yields the results for a 3-hour forecast, the different periods will be concatenated until the 48 hours of observation required are obtained.

Using the definition of storm surge as drastic changes in the force, height and amount of water it throws, it is essential to have more tide gauges on the coastline that allow establishing a measurement grid to continue refining the models. The phenomenon as such contains a large number of variables that affect its development, making it vary in strength and height by a few meters, these variables could even be the area altimetry and bathymetry.

There are other storm surge models that could be useful. The data requirements prior to their execution is what makes them unfeasible due to our technical and economic limitations; although we do not rule out its execution with the available information using "mathematical adjustments" such as interpolation.

Acknowledgment

To the Congreso Internacional Interdisciplinario de Energías Renovables, Mantenimiento Industrial, Mantenimiento e Informática (CIERMMI) 2022 and to Editorial ECORFAN-México, S.C. for allowing the development of our scientific and technical experience.

Thanks to the Secretariat of Research and Advanced Studies of the Autonomous University of the State of Mexico (Universidad Autónoma del Estado de México).

The main author is grateful for the financial support received through the postgraduate scholarship program of the Consejo Nacional de Ciencia y Tecnología (CONACYT), Mexico; reference 766292.

References

Aguilera-Méndez, J. M., Juárez-Toledo, C., Martínez-Carrillo, I., & Flores-Vázquez, A. L. (2021). Meteorological patterns recognition using Artificial Neural Networks programmed with the Swish activation function. *Revista de Tecnologías Computacionales*, *5*(15), 21–28. https://doi.org/10.35429/JOCT.2021.15.5.21.28

Aguilera-Méndez, J. M., Juárez-Toledo, C., Martínez-Carrillo, I., & Vera-Popoca, R. I. (2021). Generation of unstructured meshes using Delaunay triangles for tidal analysis of the port of Acapulco, Mexico. *Revista de Simulación y Laboratorio*, *8*(24), 20–27. https://doi.org/10.35429/JSL.2021.24.8.20.27

Aguilera-Méndez, J.M., Juárez-Toledo, C., Martínez-Carrillo, I., & Vera-Popoca, R.I. (2022). Use of unstructured meshes for wave height and particles horizontal displacement analysis in central zone Veracruz, Mexico. ECORFAN Journal-Taiwan, 6(11), 20–27. https://doi.org/10.35429/EJT.2022.11.6.20.27

Bautista, G., Orozco, R., Silva, R., & Salles, P. (2001). MODELO NUMÉRICO PARA PREDECIR INUNDACIONES POR MAREA DE TORMENTA. *Memorias Del III Congreso Internacional Puertos y Costas Retos Del Siglo XXI*.

Deftl University of Technology (TUDeftl). (n.d.). *SWAN - Simulating WAves Nearshore*. Retrieved November 30, 2022, from https://swanmodel.sourceforge.io

Delft University of Technology (TUDelft). (n.d.). *SWASH - Simulating WAves till SHore*. Retrieved November 30, 2022, from https://swash.sourceforge.io/

GEBCO Compilation Group. (2021). *GEBCO*. https://doi.org/10.5285/c6612cbe-50b3-0cff-e053-6c86abc09f8f

ISSN: 2410-3462

Global Forecast System. (n.d.). Retrieved November 30, 2022, from https://www.emc.ncep.noaa.gov/emc/pages/numerical_forecast_systems/gfs.php

Luke, R. (2006). *Mariners Weather Log* (R. A. Luke (Ed.)). Vol 50, Number 1; U.S. Departament of Commerce. https://www.vos.noaa.gov/MWL/apr_06/cover.shtml

Mcinnes, K. L., Walsh, K. J. E., Hubbert, G. D., & Beer, T. (2003). Impact of Sea-level Rise and Storm Surges on a Coastal Community. *Natural Hazards*, *30*, 187–207. https://doi.org/10.1023/A:1026118417752

Musinguzi, A., Akbar, M. K., Fleming, J. G., & Hargrove, S. K. (2019). Understanding Hurricane Storm Surge Generation and Propagation Using a Forecasting Model, Forecast Advisories and Best Track in a Wind Model, and Observed Data—Case Study Hurricane Rita. *Journal of Marine Science and Engineering*, *7*(3), 77. https://doi.org/10.3390/jmse7030077

Pecher, A., & Kofoed, J. P. (Eds.). (2017). *Handbook of Ocean Wave Energy* (Vol. 7). Springer International Publishing. https://doi.org/10.1007/978-3-319-39889-1

Rijnsdorp, D. P., & Zijlema, M. (2016). *Simulating waves and their interactions with a restrained ship using a non-hydrostatic wave-flow model*.

SEMAR. (2019). *Dirección de Meteorología*. https://meteorologia.semar.gob.mx/

WaveWatch III (WW3) Global Wave Model. (2019). https://data.noaa.gov/dataset/dataset/wavewatch-iii-ww3-global-wave-model2

World Meteorological Organization (WMO). (n.d.). *Storm Surge*. Retrieved November 29, 2022, from https://public.wmo.int/en/our-mandate/focus-areas/natural-hazards-and-disaster-risk-reduction/storm-surge

Zijlema, M. (2010). Computation of wind-wave spectra in coastal waters with SWAN on unstructured grids. *Coastal Engineering*, *57*(3), 267–277. https://doi.org/10.1016/j.coastaleng.2009.10.011

ISSN: 2410-3462

Article **Journal Simulation and Laboratory**
June 2022 Vol.9 No.26 9-17

Preparation of catalytic materials for obtaining Acrylic Acid from Ethylene and Carbon Dioxide

Preparación de materiales catalíticos para la obtención de Ácido Acrílico a partir de Etileno y Dióxido de Carbono

CANUL-CEMÉ, Carina Ivonne[1]†, CONEJO-FLORES, Ricardo[1], GARCÍA-GONZÁLEZ, Juan Manuel[1]* and GUZMÁN-PANTOJA, Javier*[2]

[1]*Universidad Autónoma de Zacatecas, Unidad Académica de Ciencias Químicas, Programa Académico de Ingeniería Química, Campus UAZ Siglo XXI.*
[2]*Gerencia de Refinación de Hidrocarburos, Instituto Mexicano del Petróleo.*

ID 1st Author: *Carina Ivonne, Canul-Cemé* / **ORC ID**: 000-0001-7091-4017

ID 1st Co-author: *Ricardo, Conejo-Flores* / **ORC ID**: 0000-0002-8513-1821

ID 2nd Co-author: *Juan Manuel, García-González* / **ORC ID**: 0000-0001-7259-5021

ID 3rd Co-author: *Javier, Guzmán-Pantoja* / **ORC ID**: 0000-0003-2103-3488

DOI: 10.35429/JSL.2022.26.9.9.17 Received March 30 2022; Accepted June 30, 2022

Abstract

The environmental problems caused by carbon dioxide emissions, as well as its accumulation in the atmosphere, have forced the scientific community to implement methods to reduce said emissions, as well as to seek alternatives for their use, one of which is in the chemical synthesis; simultaneously, catalysts with various materials that facilitate their activation have been developed. The following research paper presents the synthesis of catalysts for obtaining acrylic acid from carbon dioxide and ethylene. The materials used are transition metals: nickel and cobalt, from the salts $NiSO_4•(NH_4)_2SO_4•6H_2O$ (ammonium sulfate and nickel hexahydrate) and $CoCl_2•6H_2O$ (cobalt chloride hexahydrate). During the procedure, nickel is impregnated in a polymeric material and absorbed in a clayey material; both metals are subjected to a chemical reduction process. To verify the composition of the material, a scanning electron microscopy/X-ray energy dispersive spectrometry analysis was performed for allthe obtained materials. The results presented here are initial in the research, so the reaction to obtain the acrylic acid is not yet studied in depth. The proposed materials and gathered information are a good starting point for future research.

Carbon dioxide, Acrylic Acid, Ni and Co catalysts

Resumen

Los problemas ambientales causados por las emisiones de dióxido de carbono, así como su acumulación en la atmósfera, han obligado a la comunidad científica a implementar métodos para reducir dichas emisiones, así como buscar alternativas para su uso, donde una de estas es en la síntesis de productos químicos; de manera simultánea se han desarrollado catalizadores con diversos materiales que facilitan su activación. En el presente trabajo de investigación se detalla la síntesis de catalizadores para la obtención de ácido acrílico a partir de dióxido de carbono y etileno. Los materiales utilizados son metales de transición: níquel y cobalto, provenientes de las sales $NiSO_4•(NH_4)_2SO_4•6H_2O$ (sulfato de amonio y níquel hexahidratado) y $CoCl_2•6H_2O$ (cloruro de cobalto hexahidratado). Durante el procedimiento, el níquel es impregnado en un material polimérico y absorbido en un material arcilloso; ambos metales son sometidos a un proceso de reducción química. Para comprobar la composición del material, se realizó un análisis en el microscopio electrónico de barrido/espectrómetro de energía dispersiva de rayos X para todos los materiales obtenidos. Los resultados aquí presentados son de manera inicial en la investigación, por lo que la reacción para la obtención del ácido acrílico aún no se estudia a profundidad. Los materiales propuestos y la información recabada son un buen punto de partida para futuras investigaciones.

Dióxido de carbono, Ácido Acrílico, catalizadores de Ni y Co

Citation: CANUL-CEMÉ, Carina Ivonne, CONEJO-FLORES, Ricardo, GARCÍA-GONZÁLEZ, Juan Manuel and GUZMÁN-PANTOJA, Javier. Preparation of catalytic materials for obtaining Acrylic Acid from Ethylene and Carbon Dioxide. Journal Simulation and Laboratory. 2022, 9-26: 9-17

*Correspondence to Author (e-mail: jguzmanp@imp.mx)
†Researcher contributing as first Author.

Introduction

Due to the environmental problems caused by the constant and increasing emissions of carbon dioxide, as well as its accumulation in the atmosphere, the scientific community has seen the need to implement methods to reduce such quantities. Being an abundant and inexpensive component, one of the options that has gained interest is the use of CO_2 for the synthesis of chemical products that present high production demands; simultaneously, catalysts have been developed with different materials that facilitate their activation.

The synthesis of acrylic acid (or acrylates) from alternative routes has been gaining importance due to the increase in its production demand. An attractive option for obtaining it is the use of CO_2 and ethylene as raw materials, since, as previously mentioned, it is an economical resource, can be obtained from a wide variety of sources that present continuous emissions and is chemically stable. In addition, a wide range of catalytic systems can be employed to assist in the transformation of CO_2 into the desired product.

Acrylic acid is produced industrially by catalytic oxidation processes of propene or propylene. Following the methodology proposed by Douglas, Figure 1 shows the reactions carried out for the conceptual design of the process, through its hierarchical decomposition (Babiano, 2019).

$$C_3H_6 + \frac{3}{2}O_2 \rightarrow C_3H_4O_2 + H_2O \quad \text{R-1}$$

$$C_3H_6 + \frac{5}{2}O_2 \rightarrow C_2H_4O_2 + H_2O + CO_2 \quad \text{R-2}$$

$$C_3H_6 + \frac{9}{2}O_2 \rightarrow 3CO_2 + 3H_2O \quad \text{R-3}$$

Figure 1 Acrylic acid formation reactions from partial oxidation of propylene
(Babiano, 2019)

Initially propylene (C_3H_6) is mixed with air to react with the oxygen present and thus generate the three shown reactions, producing two oxidations in parallel to the main reaction, reactions R-2 and R-3. Reaction R-1 is the desired reaction since it generates acrylic acid ($C_3H_4O_2$).

Reactions R-2 and R-3 are considered undesirable due to the formation of by-products, acetic acid ($C_2H_4O_2$) and carbon dioxide (CO_2), although acetic acid can be sold, it has less economic value than acrylic acid, so the selectivity of acrylic acid should be one of the main parameters to be taken into account during the reaction and CO_2 should be produced in low concentrations to reduce its emissions and propylene losses.

The overall process of obtaining acrylic acid can be divided into 4 different stages (Reaction stage; Cooling and absorption stage; Separation stage; Purification stage), according to the authors (Catalá Masanet, 2020) and (Babiano, 2019), these stages can be observed in Figure 2.

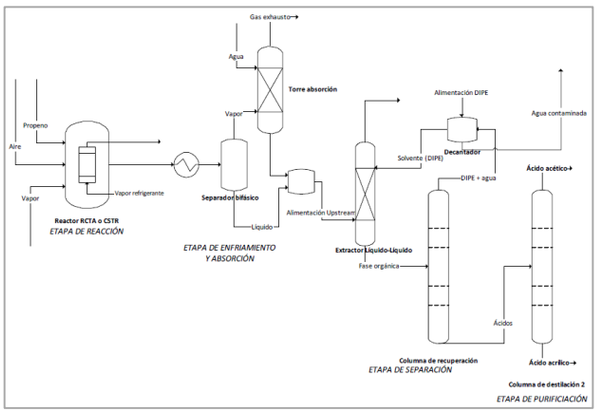

Figure 2 Diagram of the process for obtaining acrylic acid from propylene oxidation
(Catalá Masanet, 2020)

Another alternative for obtaining propylene oxidation is to selectively transform propylene into acrolein (C_3H_4O) in a first stage and then oxidize the acrolein to acrylic acid in a second stage, as described in Figure 3. Each reaction stage is carried out under different temperature and pressure conditions and exposes different catalytic systems. In the first stage, the oxidation of propylene to acrolein, the employed catalysts are multicomponent materials based on mixed oxides of MoBiO, FeSbO or SbO. In the oxidation of acrolein to acrylic acid, multicomponent catalysts based on molybdenum and vanadium oxides (Mo-V-O) are employed (Álvarado, 2019).

ISSN: 2410-3462

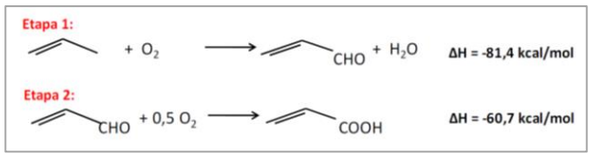

Figure 3 Oxidation reactions of propylene to produce acrylic acid mediate acrolein
(Alvarado, 2019)

In addition to the previously mentioned processes, alternative routes for the production of acrylic acid with different feedstocks from renewable sources continue to be investigated, making the process more environmentally sustainable. Of particular interest is the direct synthesis of acrylic acid from CO_2 and unsaturated hydrocarbons such as olefins/alkynes catalyzed by transition metals, as shown in Figure 4 (Yu *et al*., 2013). The oxidative coupling of CO_2 with olefins/alkynes is a procedure that has been studied quite extensively, as the first metal complex with a CO_2 molecule was isolated and characterized in 1975 (Yu *et al*., 2013).

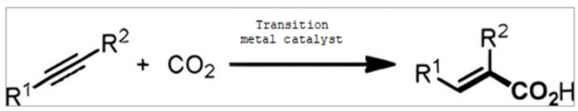

Figure 4 Synthesis of acrylic acid by carboxylation of olefins/alkynes with CO_2
(Yu et al., 2013)

Transition metals, such as nickel, are mainly used for the synthesis of compounds, where CO_2 is used as a reagent for the formation of various carboxylic acids; this is due to their different oxidation states. During the reaction, nickel forms a cyclic compound called nickel lactone; it is known that Ni (0) forms a C-C bond between CO_2 and an unsaturated molecule by oxidative cyclization (Doi & Sato, 2020). For the formation of the desired carboxylic acid to occur, an elimination of the β-hydride must be carried out, which will generate the ring opening and separation of the metal compound, as presented in Figure 5.

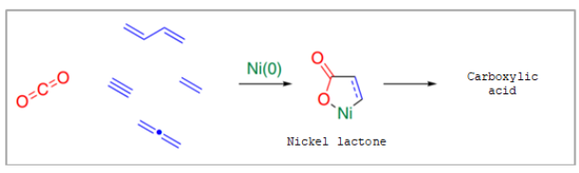

Figure 5 Formation of nickel lactone for the generation of carboxylic acids
(Doi & Sato, 2020)

The synthesis of acrylic acid from carbon dioxide (CO_2) and ethylene (C_2H_4) has always been of interest in the research field; performed studies have proposed the use of nickel-based catalysts coupled with ligands; to carry out the procedure with these materials, in the first stage, a nickel lactone must be developed that would react consequently for the generation of the compound. For the mechanism to be feasible, the ligand must produce a π-complex of acrylic acid or any other form of acrylic acid that can be used in a catalytic process (Plessow *et al*., 2014).

Other studies have shown that cobalt metal complexes present high catalytic activity, and belonging to the 3d block, they present low electronegativity that allows the formation of more nucleophilic organometallic cobalt intermediates that enable more effective reaction pathways making them good candidates for C-H bond functionalization and C-C and C-heteroatom bond formation (Cokoja *et al*., 2011).

Methodology

The methodology for the synthesis of catalysts based on ammonium nickel (II) sulfate hexahydrate ($NiSO_4•(NH_4)_2SO_4•6H_2O$) and cobalt chloride hexahydrate ($CoCl_2•6H_2O$) that will be used to obtain acrylic acid from the oxidation of carbon dioxide (CO_2) and ethylene (C_2H_4) is presented below.

Nickel with chitosan

The synthesis of the catalyst was carried out by dissolving the $NiSO_4•(NH_4)_2SO_4•6H_2O$ salt (ammonium nickel (II) sulfate hexahydrate) and impregnating it in chitosan. The procedure was carried out in an Erlenmeyer flask under constant stirring: 50 mL of distilled water and 4.25 g of the salt were placed; during this process, the pH of the solution was measured and adjusted to 5 (with the help of a solution of 0.98 M Sulfuric Acid (H_2SO_4) and 0.5 M Sodium Hydroxide (NaOH)); once the pH was reached, 1.5 g of chitosan were added and the pH was adjusted again to 5. Subsequently, the solid was filtered and washed until a neutral pH was reached (pH = 7). For drying, it was placed in a vacuum oven at 60 °C for 7 h and allowed to cool to room temperature for storage.

ISSN: 2410-3462

Nickel with Chitosan/Cloisite 10 A

As mentioned in the previous procedure, 50 mL of distilled water and 4.25 g of NiSO4•$(NH_4)_2SO_4$•$6H_2O$ (Hexahydrated Ammonium Nickel (II) Sulfate) were placed in an Erlenmeyer flask under constant stirring; once the dissolution was completed, the pH was adjusted to 5 with the same solutions of H_2SO_4 (0.98 M) and NaOH (0.5 M). The adsorption of the metal would be on the porous structure of Cloisite 10 A and chitosan.

For the preparation of the chitosan/Cloisite 10 A support, a 1% solution of acetic acid (CH_3COOH) was made (1 mL of CH_3COOH in 100 mL of water) and placed in an Erlenmeyer flask; 1.0 g of chitosan is added and left in agitation for 24 hours. After this time, a 35 ml sample of the solution is taken and placed in another Erlenmeyer flask where 0.35 g of cloisite 10 A were added and it were left stirring for 5 h. At the end of the time, the flask was introduced in an ultrasonic bath for 5 min and the content was poured in a Petri dish for drying at room temperature for 24 h. Once the material was dry, it was removed from the Petri dish and placed into a mill at medium speed; the resulting powder was placed in a beaker with 20 mL of a 5 % NaOH solution under stirring.

The new Cloisite 10 A solution was washed by filtration with distilled water until a neutral pH was reached and dried in a convection oven at 120 °C for 1 h. Once the drying was finished, it was necessary to verify that the pH did not present changes; for it, once the dry material cooled, it was placed in a beaker with 30 mL of distilled water, and it was left to rest for 1 h and a pH measurement was taken; if there was variation, more distilled water was added and it was left to rest for 48 h. Once the pH was reached, the material was filtered and left to dry for 1 h in the convection oven at 120 °C.

Next, the impregnation of the metal in the support was carried out, and for it, in an Erlenmeyer flask, an aliquot of the $NiSO_4$•$(NH_4)_2SO_4$•$6H_2O$ solution is placed together with the dry material (chitosan/cloisite 10 A) in constant stirring; once the dissolution was completed, the pH was measured and adjusted to 5 with the same acid and basic solution previously described. Finally, the resulting material was filtered and washed for drying at room temperature and storage.

Nickel with Chitosan/Cloisite 20 A

The synthesis of the chitosan/Cloisite 20 A support is carried out by taking a 35 ml sample of the 1% acetic acid solution with chitosan and adding 0.35 g of Cloisite 20 A in an Erlenmeyer flask, following the same procedure described for the Chitosan/Cloisite 10 A support. For the impregnation of the metal, the aliquot of the same $NiSO_4$•$(NH_4)_2SO_4$•$6H_2O$ solution previously prepared was taken and the described methodology was followed.

Cobalt with Chitosan

The cobalt-based catalyst was prepared with a 0.1 M (1.189 g $CoCl_2$•$6H_2O$ in 50 ml water) and 0.05 M (0.594 g $CoCl_2$•$6H_2O$ in 50 ml water) solution. Both solutions are adjusted to pH = 8 with NaOH solution (1.25 M). Once the pH is reached, 1.0 g of chitosan was added to each solution and the pH was adjusted again. The resulting solid product was washed to neutral pH and left to stand for 24 h in distilled water. After this time, if precipitate formation occurred, a series of vacuum filtrations were performed to separate the precipitate from the chitosan. After filtration, the solid was dried at 60 °C for 8 h, allowed to cool to room temperature and each resulting powder was stored.

Metal reduction with $NaBH_4$

The reduction to be carried out with $NaBH_4$ (Sodium Borohydride) was for the catalyst described in the corresponding section Nickel with Chitosan. This reaction was carried out with the objective of reducing the oxidation state of nickel from +2 to 0; for this purpose, 50 mL of distilled water and 1.90 g of $NaBH_4$ were added to an Erlenmeyer flask. Once the reagent was dissolved and hydrogen release was generated, the nickel impregnated in chitosan was added, the stirring of the solution was maintained for 6 h, at the end of the time, the metal was left to rest in the solution for 18 h. Finally, nickel was washed and filtered with chitosan for subsequent drying in a vacuum oven at 75 °C for 6 h.

ISSN: 2410-3462

Metal reduction with $LiAlH_4$

The reduction of the oxidation state of the cobalt catalysts was from +2 to 0; for this purpose, a 1 M solution of $LiAlH_4$ (1.90 g of LiAlH4 and 50 mL of Anhydrous Ether $(CH_3CH_2)_2O$)) was prepared; once the generation of hydrogen was initiated, the cobalt adsorbed on chitosan obtained in section 2.4.4 Cobalt with Chitosan was added. Stirring was maintained for 6 h and it was left in rest for 18 h. After the time elapsed, the material was filtered and dried in a vacuum oven at 30 °C for 6 h, allowed to cool to room temperature and stored.

The solutions of nickel impregnated in Cloisite 10 A and 20 A were reduced with a 1 M solution of $LiAlH_4$ (0.95 g LiAlH4 in 25 mL anhydrous ether); with the release of hydrogen, the resulting catalysts from 2.4.2 nickel with chitosan/Cloisite 10 A and 2.4.3 nickel with chitosan/Cloisite 20 A were added to their respective flask and kept in stirring for 4 h. The solution was filtered and dried in a vacuum oven at 47 °C for 4 h, allowed to cool at room temperature and stored at room temperature. Finally, it was filtered and dried in a vacuum oven at 47 °C for 4 h, allowed to cool to room temperature and stored at room temperature.

The characterization of the catalytic material was performed by Scanning Electron Microscopy and Energy Dispersive X-Ray Spectroscopy (SEM-EDS).

Results

The results of the synthesis of $NiSO_4 \bullet (NH_4)_2SO_4 \bullet 6H_2O$ (ammonium nickel (II) sulfate hexahydrate) with chitosan are presented below. Figures 6 and 7.

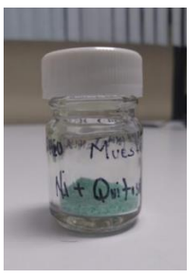

a)

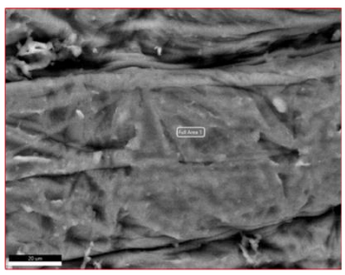

b)

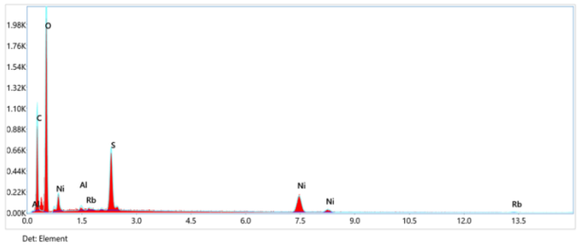

c)

Figure 6 a) Ni-chitosan based catalyst sample. b) Scanning electron microscopy of a sample of Ni-chitosan catalyst with unstable oxidation state. c) X-ray energy dispersive spectrum of a sample of Ni-chitosan catalyst with unstable oxidation state. d) X-ray energy dispersive spectrum of Ni-chitosan catalyst with unstable oxidation state

The X-ray energy dispersive spectrum (Figure 6.c) shows the presence of the elements of interest such as Nickel, Carbon, Oxygen and Sulfur (from the starting salt), as well as some Aluminum impurities.

a)

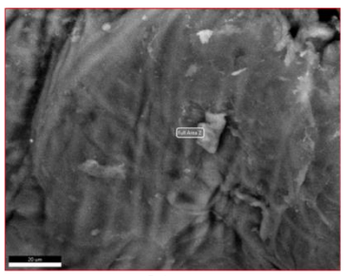

b)

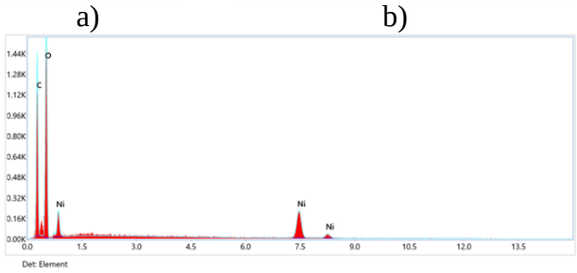

c)

Figure 7 a) Ni/chitosan-based catalyst reduced with $NaBH_4$. b) Scanning electron microscopy of a sample of Ni-chitosan catalyst with stable oxidation state.c) X-ray energy dispersive spectrum of a sample of Ni-chitosan catalyst with stable oxidation state (reduced with $NaBH_4$)

In the scanning electron microscopy of this sample (Figure 7.b), a topography similar to the previous case is observed, where color instability is present. Analyzing the preparation conditions in both samples, it can be concluded that it is important that the reduction time in the hydrogen atmosphere is long enough to achieve a stable process.

ISSN: 2410-3462

The nickel catalysts supported on chitosan and Cloisite are shown in Figure 8; their reductions were carried out in $LiAlH_4$. As with the reduction performed with $NaBH_4$, hydrogen generation was observed with the bubbling of the solution and upon addition of the dry materials, the color change was presented; the materials exhibited a paler blue-green color compared to that of nickel/chitosan, after the reaction, it changed to dark grey.

a) b)

Figure 8 Catalysts of a) Ni-Cloisite 10 A-Chitosan and b) Ni-Cloisite 20 A-Chitosan

To ensure that the reduction was maintained over time, the reaction was kept in stirring for 6 h and the solution was left to stand for 24 h, after drying, the reduced materials, 1.9958 g of powder were obtained for Cloisite 10 A and 2.5120 g for Cloisite 20 A, these samples are presented in Figure 9. In Figure 10, the X-ray energy dispersive spectra for Ni-Cloisite 10 A-chitosan and Ni-Cloisite 20 A-chitosan composites are represented. It is observed that in both cases, the presence of nickel is not detected, so it is concluded that its content is below 1% per weight.

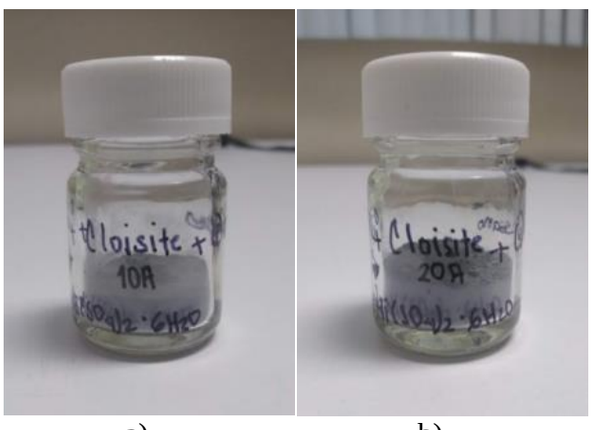

a) b)

Figure 9 Materials obtained after reduction with LiAlH4 a) Ni-Cloisite 10 A-chitosan and b) Ni-Cloisite 20 A-chitosan**.**

From the synthesis for cobalt with chitosan, 0.6592 g of 0.05 M Cobalt catalyst and 0.8153 g for 0.1 M Cobalt were obtained. During the reduction with $LiAlH_4$, the color change of the material was obtained: these presented a pale green color, with the reduction, it changed to dark gray. When the drying of the materials was finished, 5.2914 g of catalyst were obtained for the 0.05 M cobalt and 5.2363 g for the 0.1 M cobalt, these materials are presented in Figure 11.

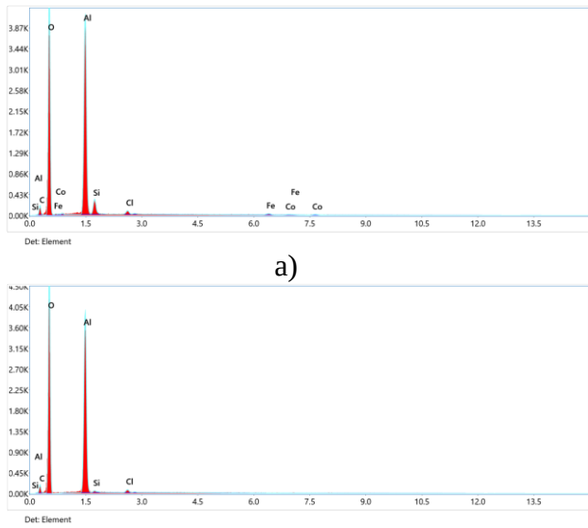

a)

b)

Figure 10 X-ray energy dispersive spectrum of a sample of the material a) Ni-Cloisite 10 A-Chitosan and b) Ni-Cloisite 20 A-Chitosan

In Figure 12, a scanning electron micrograph is observed for the cobalt-based materials; in the first one corresponding to Co (0.05 M), a value of 2.53 ± 0.4% per weight was obtained, while for Co (0.1 M), 0.8% per weight was obtained with a measurement error of 40%. As for the nickel-based catalysts, the resting time is a factor to be considered so that the reduction is constant.

a) b)

Figue 11 Materials obtained after reduction with $LiAlH_4$ a) Co (0.05 M)-Chitosan and b) Co (0.1 M)-Chitosan

ISSN: 2410-3462

Figure 13 shows the X-ray energy dispersive spectra for Co (0.05 M) and Co (0.1 M); for Co (0.1 M), the presence of cobalt is not observed, which indicates that the content in the sample is less than 1% per weight. In both cases, traces of aluminum derived from the reduction and chlorine from the respective salt are present.

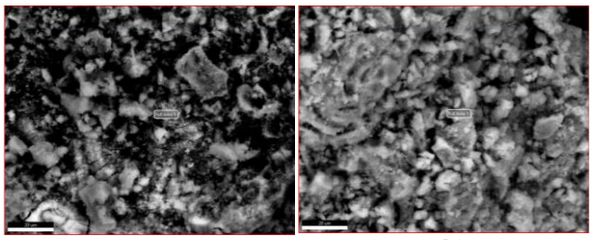

a) b)

Figure 12 Scanning electron microscopy of a sample of a) Co (0.05 M)-Chitosan and b) Co (0.1 M)-Chitosan catalysts, reduced with $LiAlH_4$

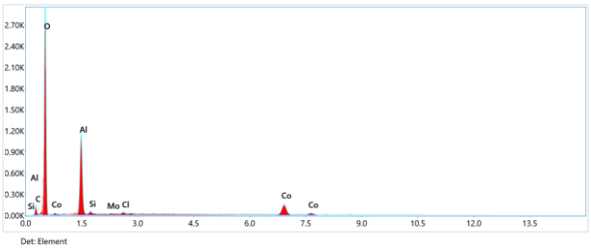

a)

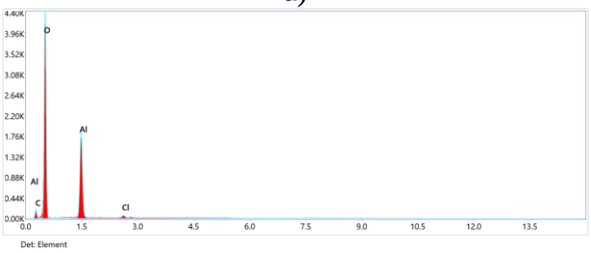

b)

Figure 13 X-ray energy dispersive spectrum of a sample of a) Co (0.05 M)-Chitosan and b) Co (0.1 M)-Chitosan catalysts, reduced with $LiAlH_4$

Analysis and Discussion of Results

The impregnation of the metals in chitosan and Cloisite was done with the objective of improving the thermal tolerance of the catalysts, because the reaction to produce the acrylic acid (or acrylates) was carried out at high temperatures since these can decompose during the reaction or before reaching the desired conversion. Chitosan and Cloisite acted as a coating for the metal without altering the properties and catalytic activity of the metal within the structures; at the same time, the latter increased the surface area as if it were a clay material, which provided more active sites for the reaction to take place.

The addition of these materials allowed the reaction to be carried out under the necessary conditions of temperature and pressure.

According to previous research works and information gathered about the behavior of LiAlH4, after the reduction reactions, it usually generates a residual sludge because part of the aluminum present does not dissolve; this behavior may explain the increase of mass in the catalysts after the performed reductions. The produced residue was eliminated according to the amount generated and in proportion to the amount of reduced material. The mechanism chosen to carry out the elimination does not usually affect the properties of the involved substances.

The reductions carried out with NaBH4 in comparison with those carried out with $LiAlH_4$ did not preserve the color change after the drying time, for this reason the contact time with the reducing solution was extended to 24 h, this modification only worked for the nickel catalyst impregnated in chitosan. During the reduction process, this was only checked qualitatively by means of the color change; since no measurements were made with other parameters during the procedure, there was uncertainty in the results, since a metal can be reduced without presenting a change in its original color.

The resting time in the hydrogen medium was a very important factor in the reductions for both reducing substances, as the results showed that the longer the contact time, the more constant and stable the reduction after the drying period.

To confirm the reduction of a metal in a quantitative and accurate way, it is necessary to measure several physicochemical parameters such as pH and the electrical potential of the solution, to mention a few. The characterization of the dried materials was also carried out using scanning electron microscopy and X-ray energy dispersive spectra; the latter allow very precise verification of the chemical composition, structure and distribution of the materials, as well as the presence of residual substances.

ISSN: 2410-3462

As mentioned, for the metals present in the samples to appear in the images obtained by SEM-EDS, they must be present in a composition of 1% per weight; in the case of the Co catalyst (0.1 M), the metal of interest does not appear in the X-ray energy dispersive spectroscopies, which helps to deduce that the percentage per weight is below the required one; traces of Al from the $LiAlH_4$ and Cl from the $CoCl_2 \bullet 6H_2O$ salt can be observed. During the synthesis of the material, the formation of the precipitate is mentioned and consequently the washing and filtering of the precipitate, during this process the loss of Co can occur. In comparison with the synthesis of Co (0.05 M) for this concentration, there was no precipitate formation and the presence of cobalt was higher in the different areas analyzed.

The energy dispersive X-ray spectroscopies for the Ni-chitosan-Cloisite 10 A and 20 A based catalysts show similar results to those of Co; the absence of Ni in the spectra indicates that its content is less than 1 wt.%, traces of Al from the reduction are observed and even Cloisite components such as Si, Fe and Mg are present. In the Ni-chitosan catalyst sample, the spectroscopies indicate the presence of Ni and S corresponding to the salt with which it was worked ($NiSO_4 \bullet (NH4)_2SO_4 \bullet 6H_2O$). For the sample of Ni-chitosan reduced with $NaBH_4$, samples were obtained free of impurities, unlike those reduced with $LiAlH_4$, in addition to the fact that no signals of the reducing agent are present.

Conclusions

The catalysts were obtained from the salts of cobalt chloride hexahydrate and ammonium nickel sulfate, with the reduction of the corresponding metal centers. The adsorption of nickel on chitosan and the impregnation on Cloisite 10 A and 20 A were verified by pH measurements during dissolution, the series of washes and after the drying time had elapsed. To perform the reduction of the metallic center of the catalysts, the contact time of the materials with the reducing substance was a determining factor for its success. The characterization of the materials helped to verify the presence of the substances of interest in the resulting materials, since aluminum is present in the X-ray energy dispersive spectroscopies of all the samples, where $LiAlH_4$ was used, it is proven that it is the element that caused the increase in the mass of the catalysts.

In addition, compared to the reduction performed with NaBH4, the spectra of the Ni-chitosan samples did not show the presence of sodium or boron (remembering that it must have 1% per weight to present a signal); therefore, the existence of traces of these elements is insignificant.

Since the mechanism to obtain Acrylic Acid with the proposed reagents and the synthesized catalysts was not proposed, the methodology to carry out the reaction is open to future researche covering the process in a complete way. In order to obtain the desired product, the search for catalysts with different transition metals, impregnation materials and synthesis methods that help the process to be successful must be expanded; therefore, the proposed materials work as a good starting point for such investigations.

References

Álvarado, C. Oxidación Parcial de Propileno sobre Catalizadores Basados en Óxidos Mixtos de Mo-V-Te-Nb. Tesis de Maestría. Universidad Politécnica de Valencia, Valencia, España, 2019.

Babiano, L. Diseño del Proceso de Producción de Ácido Acrílico e Impacto Económico del Diseño del Reactor. Tesis de Licenciatura. Universidad Politécnica de Madrid, Madrid, 2019.

Catalá Masanet, J. L. Diseño de un Proceso de Producción de Ácido Acrílico, Vía Acroleína. Tesis de Licenciatura, Universidad Politécnica de Valencia, Valencia, España, 2020.

Cokoja, M.; Bruckmeier, C.; Rieger, B.; Herrmann, W. A.; Kühn, F. E. Transformation of Carbon Dioxide with Homogeneous Transition-Metal Catalysts: A Molecular Solution to a Global Challenge? *Angew. Chem. Int. Edit.*. 2011, 50 (37), 8510-8537. DOI: 10.1002/anie.201102010.

Doi, R.; Sato, Y. Carbon Dioxide Fixation via Nickelacycle. In *Nickel Catalysis in Organic Synthesis: Methods and Reactions*, Osaka, University 2020, pp 249-283. DOI: https://doi.org/10.1002/9783527813827.ch11.

ISSN: 2410-3462

Plessow, P. N.; Schäfer, A.; Limbach, M.; Hofmann, P. Acrylate Formation from CO2 and Ethylene Mediated by Nickel Complexes: A Theoretical Study. *Organometallics*. 2014, 33 (14), 3657-3668. DOI: https://doi.org/10.1021/om500151h.

Yu, B.; Diao, Z.-F.; Guo, C.-X.; He, L.-N. Carboxylation of olefins/alkynes with CO_2 to Industrially Relevant Acrylic Acid Derivatives. *J. CO_2 Util.* 2013, 1, 60-68. DOI: https://doi.org/10.1016/j.jcou.2013.01.001

ISSN: 2410-3462

Article **Journal Simulation and Laboratory**
June 2022 Vol.9 No.26 18-30

Simulation of gas condensation process from pyrolysis of used tires

Simulación del proceso de condensación de gases de la pirólisis de neumáticos usados

MORENO-ARIAS, Claudio Alberto[1]†*, CHAMARRAVÍ-GUERRA, Oscar[2] and LOPÉZ-MAZA, Fernando de Jesús

Fundación Universidad de América, Facultad de Ingenierías, Bogotá D.C., Colombia

ID 1st Author: *Claudio Alberto, Moreno-Arias* / **ORC ID**: 0000-0001-6103-8238

ID 1st Co-author: *Oscar, Chamarraví-Guerra* / **ORC ID**: 0000-0002-6571-6814

ID 2nd Co-author: *Fernando De Jesús, Lopéz-Maza* / **ORC ID**: 0000-0002-1711-4739

DOI: 10.35429/JSL.2022.26.9.18.30 Received March 30 2022; Accepted June 30, 2022

Abstract

Waste tires, composed of rubber, have caused negative environmental problems. There have been problems regarding an increase in the accumulation of tires in different sectors, together with the fact that waste management methods are obsolete. These problems have awakened interest in their study and thermal degradation. Tires composed of rubber represent a material with an important potential for recycling and utilization, together with the conversion of these wastes into energy, value-added products or for the improvement of raw materials. The technique used to carry out thermal degradation is called pyrolysis and consists of heating the organic matter in the absence of oxygen at a specified rate or heating rate, up to a maximum temperature known as pyrolysis temperature, and maintaining it there for a specified time. The products of pyrolysis correspond to: liquid, condensable gases and solid char or ash; for its part, the condensable gas can be further decomposed into non-condensable gases (⟦CO, CO_2, H_2 and CH_4), liquid and char. This work aims to contribute with the design and simulation of the condensation cycle of the gases obtained from pyrolysis. Particularly, for the condensation of these gases, the ASPEN HYSYS process simulator was used, where the adaptation of a shell and tube heat exchanger allowed to carry out the condensation. The feed containing these gases comes from tests in a pyrolytic reactor with favorable results. As a result of this condensation and the operating conditions, it is observed that, for a range between 80 and 90 °C, the condensation of gases such as i-Butene and Propylene is favored. This study aims to take up existing research in this area and make a proposal for the condensation of pyrolysis gases, generating an idea of the feasibility and recovery of tire waste with a circular economy approach.

Recycling, Waste, Tires, Pyrolysis, Condensation

Resumen

Los neumáticos de desecho, compuestos por caucho, han causado problemas ambientales negativos, se han registrado problemáticas respecto a un aumento en la acumulación de llantas en diferentes sectores aunado a que los métodos de gestión de los residuos son obsoletos. Estos problemas han sido tan evidentes que han despertado el interés para su estudio y la degradación térmica de estos mismos. Las llantas compuestas por caucho representan ser un material con un potencial importante para el reciclaje y su aprovechamiento, aunado a la conversión de estos desechos en energía, productos de valor agregado o para la mejora de materias primas. La técnica por la cual se lleva a cabo esta degradación térmica se denomina pirólisis y consiste en calentar la materia orgánica en ausencia de oxígeno a una velocidad especificada o tasa de calentamiento, hasta una temperatura máxima conocida como temperatura de pirólisis, y mantenerla allí durante un tiempo especificado. Los productos de la pirólisis corresponden a: líquido, gases condensables y carbón sólidos o ceniza; por su parte, el gas condensable puede descomponerse aún más en gases no condensables (CO, CO_2, H_2 *y* CH_4), líquido y carbón. Este trabajo tiene como objetivo contribuir con el diseño y simulación del ciclo de condensación de los gases obtenidos de la pirólisis. Particularmente, para la condensación de estos gases, se emplea el simulador de procesos de ASPEN HYSYS en donde se realiza la adaptación de un intercambiador de calor de tubo y coraza que permitirá llevar a cabo la condensación. La alimentación que contiene a estos gases es proveniente de pruebas en un reactor pirolítico con resultados favorables. Resultado de esta condensación y de las condiciones de operación se observa que, para un rango entre 80 y 90 °C, se favorece la condensación de gases como lo son el $i-Buteno$ y el $Propileno$. Este estudio pretende retomar las investigaciones existentes en este rubro y realizar una propuesta para la condensación de los gases de pirólisis, generando una idea de la viabilidad y la valorización de residuos de llantas con un enfoque de economía circular.

Reciclaje, Residuos, Llantas, Pirólisis, Condensación

Citation: MORENO-ARIAS, Claudio Alberto, CHAMARRAVÍ-GUERRA, Oscar and LOPÉZ-MAZA, Fernando de Jesús. Simulation of gas condensation process from pyrolysis of used tires. Journal Simulation and Laboratory. 2022, 9-26: 18-30

*Correspondence to Author (e-mail: claudio.moreno@profesores.uamerica.edu.co)
†Researcher contributing as first Author.

Introduction

Tires composed of rubber are materials with a growing negative environmental impact, both for the city of Bogotá and for the country itself; according to the statements of Cardona-Gómez and Sánchez-Montoya [1], 1% of the total waste generated in Colombia comes from rubber. In the work carried out by Castillo-Viveros and Simancas-Robles [2] it is highlighted that, in the City of Bogotá, there have been problems regarding an increase in the accumulation of tires in different sectors and their final disposal. Furthermore, in 2016, Durán [3] states that around 30 million tires were discarded in the country and, particularly in Bogotá, an estimated 4 million in that year alone. Rubber waste is a major global concern, due to its slow decomposition, which is estimated that outdoors this process takes between 500 and 3000 years [2]. Waste management methods are obsolete, based on combustion or accumulation in landfills, clandestine deposits, residential yards or even public spaces, also due to the high elasticity of tires that impairs their compaction.

The increase in vehicle use has accumulated thousands of tons of waste, which can cause the accumulation of gases that can lead to fires, generation and spread of pests and diseases that represent a risk to public health. Therefore, rubber tires used in automobiles are an excellent example of a material that, although historically is not biodegradable, its main components are rubber (a cross-linked styrene-butadiene), steel cords and other organic and inorganic compounds [4].

These represent a material with an important potential for recycling and utilization. Likewise, the conversion of these wastes into energy, value-added products or for the improvement of raw materials, should be a sustainable way that allows the best use of these wastes and thus, they go from being a waste or a problem to a product with a particular interest attached to the regulations in force.

The Colombian state through Resolution No. 1457, issued on July 29, 2010, establishes that some subsectors use used tires as fuel in their production processes, but this inadequately, others burn them in the open air for the extraction of steel, one of the components of tires, this is a polluting source for the atmosphere and also for human health.

In addition to the above, this resolution aims to properly manage the waste from used tires, highlighting the responsibility of manufacturers and producers of these and emphasizing that it is a task that requires awareness campaigns, both manufacturers and people who have a vehicle. If tire demand and production increase, sales increases and, as a consequence, tire waste and its accumulation also increases According to Castellanos [5], there are three main thermochemical processes: combustion, gasification and pyrolysis. As mentioned by Bolivar and Cuenca [6], combustion can be defined as the total oxidation of a fuel to produce energy; gasification is the total degradation of the carbon substrate to gaseous form; the third of these main processes is pyrolysis and, as mentioned, it is the transformation of biomass into liquid, solid and gaseous fractions generated by heating the biomass, in the absence of oxygen, and with temperatures close to 500 °C.

As mentioned above, pyrolysis consists of heating organic matter in the absence of oxygen at a specified rate or heating rate, up to a maximum temperature known as pyrolysis temperature, and maintaining it there for a specified time [6]. The products of pyrolysis correspond to: liquid, condensable gases and solid char or ash; in turn, the condensable gas can be further decomposed into non-condensable gases (CO, CO_2, H_2 and CH_4), liquid and char [7]. This process is gaining its place as a suitable recycling technique and can be carried out in different ways depending on a combination of the operating conditions, the nature of the reactor employed or even the use or not of a catalyst; it is important to note that this is a process that demands heat energy for the thermal degradation reactions to take place.

The products obtained from the pyrolytic process are three, mainly the solid product (ash or carbon black), the liquid product (oil) and the gaseous product, which contains condensable and non-condensable gases. According to Castells and Velo [8], the pyrolytic product is made up of smaller molecules that are separated from the carbon chains of the biomass, in this particular case rubber; i.e. from one to four carbon compounds such as methane (CH_4), propane ($C_3 H_8$) and butane (C_4H_{10}); in addition to non-pyrolytic gases such as hydrogen (H_2), carbon dioxide (CO_2) and carbon monoxide (CO).

ISSN: 2410-3462

By the end of the 2030s, the weight of scrap tires will be up to 1200 million tons annually [9], [10]. Currently, this particular process proves to be a promising way for the transformation of waste organic matter, such as tires consisting mainly of rubber, into fuel by thermal degradation in the absence of oxygen in a temperature range from 300 to 800 °C.

The present research article will focus on the valorization of tire waste with a circular economy approach, particularly on the design and simulation of the tire pyrolysis gas condensation process to obtain crude oil for liquid fuels. The input variables for the pyrolytic gas condensation process will be identified and the simulation model that allows the condensation of these gases from the pyrolysis reactor will be developed.

1. Materials and Methods

1.1 Description of the process

Scrap tires, which mainly consist of rubber, are an important alternative for obtaining energy, due to their main composition in the form of CxHy with a calorific value of 33 MJ/kg [11]. In addition, they are the raw material that constitutes the pyrolysis of tires. This process produces more than 110 products according to experimental results obtained from oil and gas industries, and they can be identified as gas, non-aromatic liquids, aromatic liquids and tar at 530 °C, the process presents three stages of thermal decomposition between 120 and 520 °C, which corresponds to the volatilization of plasticizers and degradation of natural and synthetic rubber [12].

Pyrolysis is an alternative for the conversion of tires into energy; it consists of the thermal decomposition of macromolecules in the absence of oxygen to obtain products such as liquids, gases and residual carbon that can be used as raw materials for other processes or as fuels [13], [14], [15]. Coal can be used as a solid fuel or can be converted into activated carbon. Gas, which mainly consists of butadiene, ethylene and methane, with its high calorific value can be used as an energy source again for the process.

The oil contains high value-added and commercially valuable components such as benzene, toluene, xylenes and limonene. For this process, variables and operating conditions are defined and from this the experimental stage can be developed.

The feed to the ASPEN HYSYS model has been characterized as a mixture of gases coming from the pyrolysis reactor, in its experimental stage, with a composition taken from a gas chromatography carried out previously [6].

1.2 Experimental design

Tires go through a pretreatment where the main objective is the size reduction of the samples into smaller pieces, up to dimensions close to 4 x 4 cm, these are the starting point of the pyrolysis process. Subsequently, the samples enter a reactor that has been adapted with recycled and reused material as illustrated below:

Figure 1 Pyrolysis reactor
Source: Own Elaboration

A burner provides heat to the reactor, which operates at 1 atm pressure, the corresponding temperature measurements are taken and, subsequently, the pyrolysis gas leaves the reactor to enter a shell and tube heat exchanger that has a tube bundle of 21 tubes in a single pass, in a square layout.

This functions as a condenser and employs a countercurrent water flow as the cooling fluid. The water is pumped to the exchanger by a 0.5 hp water pump as shown in figures 2 and 3.

ISSN: 2410-3462

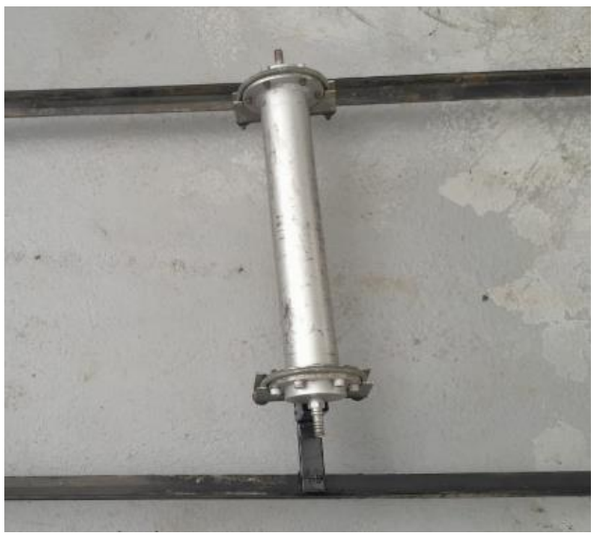

Figure 2 Shell and tube heat exchanger
Source: Own Elaboration

Figure 3 Water pump
Source: Own Elaboration

The water is recirculated back to the water pump, at the outlet of the heat exchanger the condensed gas is obtained. Considering that cooled gas is not completely condensed, the remaining is recirculated to the burner as a power source. The assembly of the equipment is illustrated below:

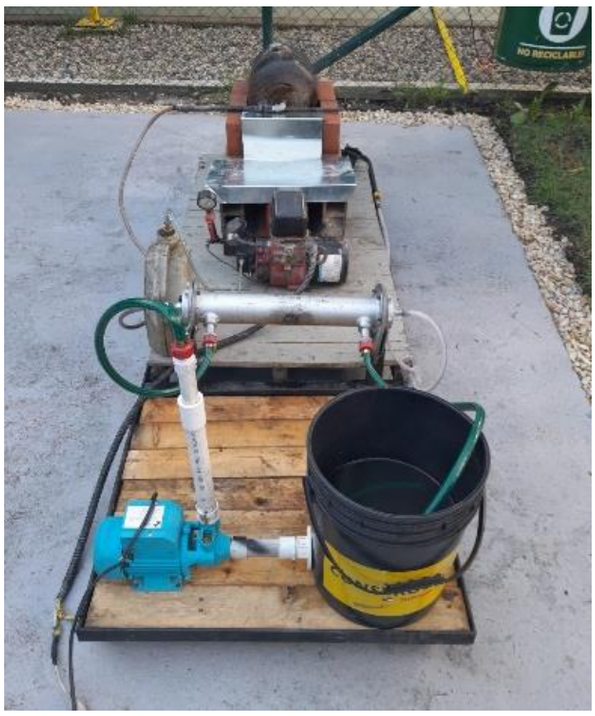

Figure 4. Rubber pyrolysis equipment
Source: Own Elaboration

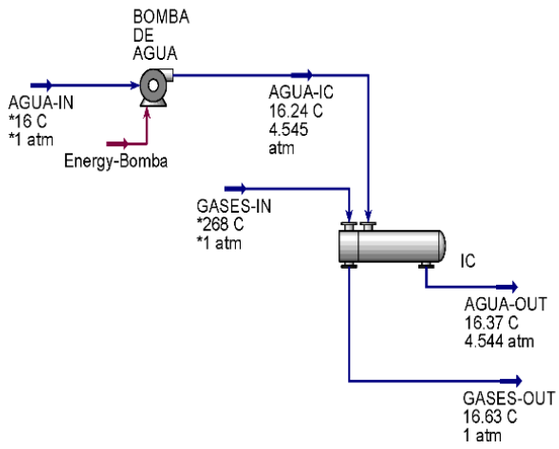

Figure 5 Flow process diagram
Source: Own Elaboration

1.3 Model description

The process flow diagram, elaborated in the ASPEN HYSYS simulation software, corresponds to the cooling cycle with the objective of condensation of the gases coming from the pyrolysis reactor, it consists of a water pump and a shell and tube heat exchanger; the efficiency, power, in the case of the pump, the dimensions of both the tubes and the shell and its length, for the heat exchanger, have been taken from the equipment mentioned in the experimental stage.

ISSN: 2410-3462

According to Acosta and Castro, among the variables that most influence the pyrolysis process are the type of biomass to be fed into the reactor, in this case tires, the time-temperature profile and the atmospheric pressure, the latter two being the most important, together with the particle size and moisture level. As for the time-temperature profile, it refers to the heating rate, the maximum temperature and the residence time [17]. Having said that, by correctly managing the process variables mentioned above, it is possible to optimize or, if necessary, maximize the fraction of the desired product.

1.3.1 Feed gas composition

To determine the composition of feed gas, which is a gaseous mixture, a gas chromatography is used to separate the different volatile compounds of a gaseous sample in this case. This technique achieves the separation of these compounds with the passage of a sample through a stationary phase with help of a mobile phase; in addition, it allows to know both the absence or presence of a compound, as well as the amount of individual components present in a sample through the calibration curves of each standard, likewise it has a great capacity for separation of both thermally stable and volatile organic and inorganic compounds [16].

The composition of the feed gas, the chemical compounds in (% mol) of the synthesis gas from the tire rubber pyrolysis process at different temperatures resulting from the samples selected for chromatographic analysis performed previously [6] are:

Process temperature (°c)			
Components	400	450	500
H_2	8	9.1	11.6
CH_4	20.3	21.8	27.5
CO	4.5	2.7	3.1
CO_2	5.8	5.2	4.6
C_2H_4	9.2	9.9	9.1
C_2H_6	6.6	8.6	10.6
H_2S	0.9	1.3	1
C_3H_6	6.5	6.3	5.7
C_4H_8	31.8	27.2	19
Others	6.4	7.9	7.8

Table 1 Chemical compounds in (%mol) of the synthesis gas from the tire rubber pyrolysis process at different temperature
*Source: LEONARDI, Chiara. Development of an innovative pyrolysis plant for the production of secondary raw materials. Dottorato di ricerca in chimica .Università di Bologna. 2015 *Diferentes tipos de neumáticos*

These gases together with their corresponding mole fraction are entered as the feed components through the shell and tube heat exchanger tubes. In addition, the cooling liquid of choice is water which enters the shell side of the heat exchanger with a mole fraction of 1. In the ASPEN HYSYS simulator they are categorized at 1 atm pressure as follows:

Formula	Simulation Name	Molar Fraction
H_2	Hydrogen	0.08
CH_4	Methane	0.203
CO	CO	0.045
CO_2	CO_2	0.058
C_2H_4	Ethylene	0.092
C_2H_6	Ethane	0.066
H_2S	H_2S	0.009
C_3H_6	Propene	0.065
C_4H_8	i-Butene	0.318
Others	Others	0.064

Table 2 Chemical compounds present in the feed to the simulation in ASPEN HYSYS
Source: Own Elaboration

Likewise, in the experimental stage, the corresponding temperature gases (hot fluid), as well as for the water (cold fluid) were measured; The mass flow of gas feed and the volume flow of water before entering the pump that feeds the heat exchanger were measured as well; in addition, it is important to highlight the process is carried out at 1 atm of pressure. These conditions are listed below:

Fluids		
Parameters	Water	Pyrolysis gases
Inlet temperature (°C)	16	268
Mass flow rate $\left(\frac{kg}{h}\right)$	-----	1
Flow rate $\left(\frac{L}{min}\right)$	16.39	-----

Table 3 Feed parameters to the process at 1 atm pressure obtained from the experimental stage
Source: Own Elaboration

The above mentioned compositions and feed parameters are the starting point of the simulation performed in ASPEN HYSYS and will allow the process to be carried out.

1.3.2 Properties

The equation-of-state models provide an accurate description of the thermodynamic properties of the high temperature conditions for the pyrolysis gases coming from the reactor, for the hot side entering through the heat exchanger tubes.

ISSN: 2410-3462

The Peng-Roninson model was chosen for this application because of the majority of hydrocarbon gas components. For the cold side of the heat exchanger, which enters through the shell of the heat exchanger, the NRTL model was chosen because water is a polar compound and enters at a pressure of less than 10 bar. The normal boiling points (°C) of the components are listed below according to the ASPEN HYSYS simulator where the components have been normalized.

Formula	Simulation Name	Molar Fraction	Normal Boiling Pt (°C)
H_2	Hydrogen	0.0855	-252.6
CH_4	Methane	0.2169	-161.5
CO	CO	0.0481	-191.5
CO_2	CO_2	0.0620	-78.55
C_2H_4	Ethylene	0.0983	-103.8
C_2H_6	Ethane	0.0705	-88.60
H_2S	H_2S	0.0096	-59.65
C_3H_6	Propene	0.0694	-47.75
C_4H_8	i-Butene	0.3397	-6.851

Table 4. Boiling points of feed components according to ASPEN HYSYS
Source: Own Elaboration

1.3.2 Components of the simulation

The simulation is comprised of two main pieces of equipment, the water pump which will receive a flow rate of 16.39 L/min and, in turn, the output of this equipment will feed the shell and tube heat exchanger.

1.3.2.1 Water Pump

This equipment increases the pressure of a liquid stream; it calculates pressure, temperature or efficiency. It is part of the experimental stage and its main characteristics, which have been entered into the process simulator, are mentioned below:

Water pump	
Parameters	Specifications
Inlet temperature (°C)	16
Inlet flow rate $\left(\frac{L}{min}\right)$	16.39
Adiabatic efficiency (%)	25.90
Duty (hp)	0.5

Table 5 Water pump specifications
Source: Own Elaboration

1.3.2.2 Heat Exchanger

The heat exchanger transfers heat between two streams; the reactor outlet gas is cooled with water coming from the pump entering countercurrent. The hot fluid, the gas, enters this device through the tubes and the cold fluid, the water, through the shell. This heat exchanger has been adapted from another cooling process and its specifications are described:

Type of heat exchanger	AEL
Position	Horizontal
Shell outer Diameter (DO)	0.06604 m
Shell Internal Diameter (DI)	0.05267 m
Number of tubes	21
Length of tubes	0.50 m
Number of passages through tubes	1
Outer diameter of tubes (DO)	0.00793 m
Inner diameter of tubes (DI)	0.00663m
Tube spacing (PT)	0.00992 m
Tube pattern (arrangement)	Cuadrado 90 °
Outer diameter (OD) and inner diameter (ID) of nozzle where fluids enter	21.34/16.6 mm

Table 6 Shell and Tube Heat Exchanger Specifications
Source: Own Elaboration

With the specifications mentioned above, the layout of the heat exchanger itself and the pattern of the tubes are constructed in the simulator:

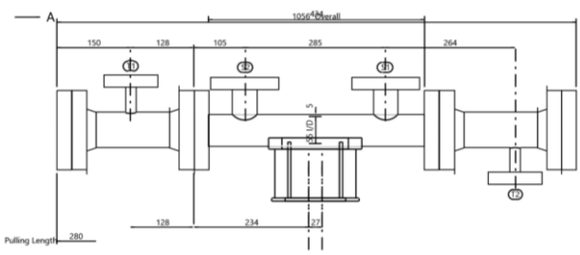

Figure 6 Layout of the heat exchanger
Source: Own Elaboration

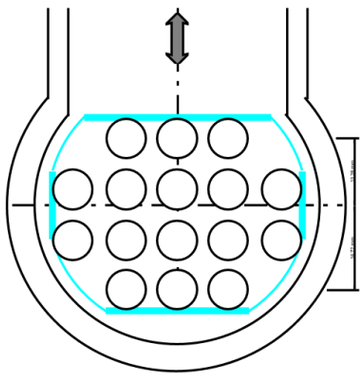

Figure 7 Square arrangement of the tubes
Source: Own Elaboration

ISSN: 2410-3462

Having said that, the above mentioned parameters and operating conditions are entered into the simulation in ASPEN HYSYS and the model is allowed to run. The simulation results will be shown in section 3.

1.4. Use of refrigerant R-717

An alternative in the cooling system is the use of a refrigerant, in this case R-717, the simulation illustrated in Figure 5 is taken up again and the cold fluid feeding the process is varied, replacing in this case water to observe if this favors the condensation of the pyrolysis gases coming from the reactor in the experimental stage.

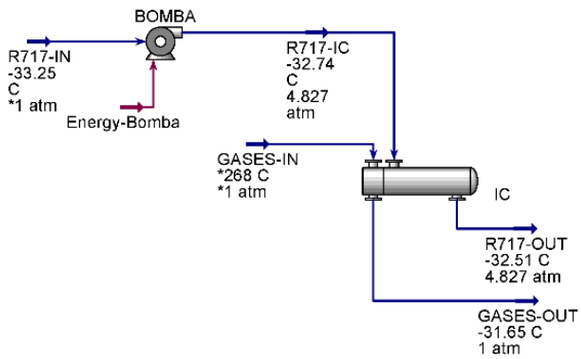

Figure 8 Refrigerant process diagram
Source: Own Elaboration

1.4.1 Characteristics of the refrigerant R-717

The coolant enters in liquid phase and with a mole fraction of 1, the characteristics of the feed at 1 atm of pressure are listed in the following table:

R-717 refrigerant	
Parameters	Especifications
Inlet temperature (°C)	-33.25
Inlet flow rate$\left(\frac{L}{min}\right)$	16.39

Table 7 R-717 refrigerant specifications at 1 atm pressure
Source: Own Elaboration

2. Results and discussion

2.1. Simulation results

Based on a pyrolysis gas feed to the process of 1 kg/h, the results obtained in the simulation are listed:

Water pump		
Delta P	3.545	atm
Power	0.5	hp
Efficiency	25.90	%
Inlet pressure	1.000	atm
Outlet Pressure	4.545	atm
Flow rate	16.39	L/min
Inlet Temperature	16	°C
Outlet temperature	16.24	°C

Table 8 Water pump results in ASPEN HYSYS
Source: Own Elaboration

The above describes that the cold fluid, water, enters the shell of the heat exchanger with a pressure of 4.545 atm and a temperature of 16.24 °C; that is, the water pump provides an increase in pressure and a slight increase in temperature to the water. According to the composition of the gas mixture fed to the process and taken from the literature, the pertinent analysis of the heat exchanger is carried out, which provides the following results:

Shell & tube heat exchanger					
		Shell		Tubes	
Process data	Units	Input	Output	Input	Output
Total flow	$\frac{kg}{h}$		981		1
Steam	$\frac{kg}{h}$	0	0	1	1
Líquid	$\frac{kg}{h}$	981	981	0	0
Temperature	°C	16.24	16.37	268	16.62
Vapor mass fraction		0	0	1	1
Pressure	KPa	460.534	460.387	101.325	101.321
Convection coefficient	$\frac{W}{m^2 \cdot K}$		774.8		16.6
Duty	kW				0.1381
Area	m^2				0.2296
UA	$\frac{kJ}{°C \cdot h}$				11.4
LMTD	$°C$				43.62

Table 9 Heat exchanger results using water provided by ASPEN HYSYS
Source: Own Elaboration

The temperatures of both the hot fluid, in red, and the cold fluid, in blue, along the path through the heat exchanger are illustrated in the graph below. It is possible to observe the cooling that the hot fluid undergoes from a feed temperature of 268 °C to its exit from the heat exchanger at 16.63 °C. In addition to the above, the water undergoes a slight heating from its exit from the pump and entrance to the heat exchanger on the shell side, with a temperature of 16.24 °C until it exits at 16.37 °C.

ISSN: 2410-3462

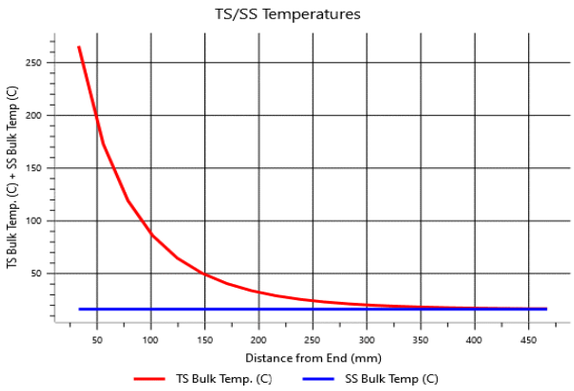

Figure 9 Temperature profile using water
Source: Own Elaboration

It also illustrates the slight pressure drop that occurs on the tube side of the heat exchanger, along the 500 mm distance that the gases have to travel against the flow of water fed to the process by means of the centrifugal pump. The above has been calculated by the simulator itself.

Figure 10 Pipe side pressure drop
Source: Own Elaboration

In addition to the above, the film or convection coefficients for both fluids are presented, in blue the coefficient of the cold fluid, water, and in red the hot fluid, pyrolysis gases, this coefficient quantifies the influence of the properties of the fluid, surface and flow when heat transfer by convection occurs and that, contrasted with Table 9, have a value of 774.8 and 16.6 W/(m^2· K), respectively.

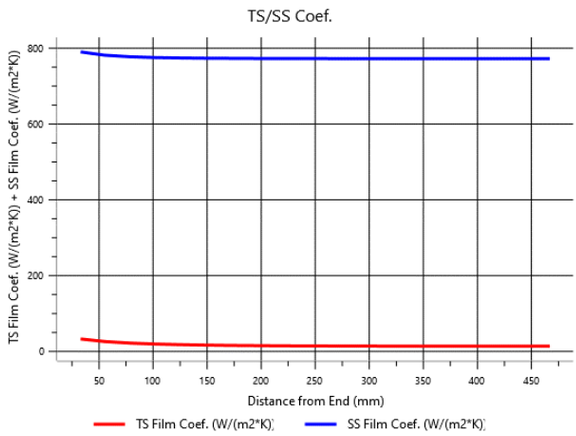

Figure 11 Film coefficients of both fluids
Source: Own Elaboration

Finally, to determine whether the gases that make up the feed have condensed, taking into account that the components of this mixture, as well as their mole fraction composition, have been taken from the literature as mentioned in Table 2, the following graph is observed. It illustrates the mole fraction of the gas mixture against the length of the shell and tube heat exchanger itself.

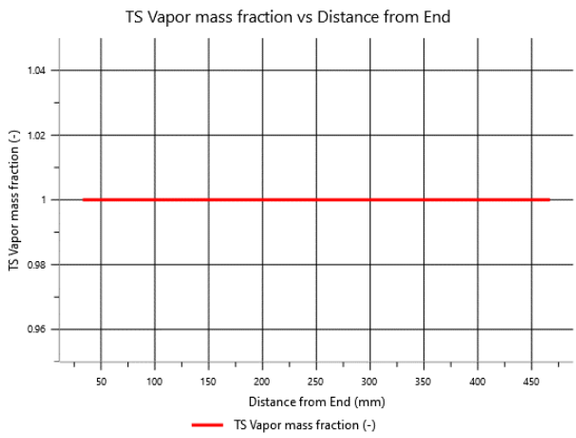

Figure 12 Fraction of steam in the heat exchanger
Source: Own Elaboration

According to the above graph, no condensate formation is observed for this gas mixture mentioned in Table 2 and entered into the ASPEN HYSYS simulator, when water is used as the cooling liquid, this is supported by the phase change temperatures listed in Table 4. For more accurate results for this particular process, it is recommended to perform a gas chromatography on the gas mixture coming directly out of the pyrolysis reactor, which favors the determination of the chemical compounds and their molar compositions present in the gas stream.

ISSN: 2410-3462

With the above, the mole fractions of the components of the hot fluid leaving the heat exchanger are listed, all of them in vapor phase:

Formula	Simulation Name	Molar Fraction
H_2	Hydrogen	0.0855
CH_4	Methane	0.2169
CO	CO	0.0481
CO_2	CO_2	0.0620
C_2H_4	Ethylene	0.0983
C_2H_6	Ethane	0.0705
H_2S	H_2S	0.0096
C_3H_6	Propene	0.0694
C_4H_8	i-Butene	0.3397

Table 10 Mole fractions of the gaseous stream at the heat exchanger outlet
Source: Own Elaboration

2.2. Results of the use of R-717 refrigerant

As mentioned above, the use of R-717 refrigerant is an alternative to favor the condensation of the pyrolysis gases that make up the gaseous mixture at the outlet of the pyrolysis reactor and that enters the heat exchanger on the side of its tubes. The results are listed for the pump that will feed the cooling fluid.

PUMP		
Delta P	3.827	atm
Power	0.5	hp
Efficiency	25.90	%
Inlet pressure	1.000	atm
Outlet pressure	4.827	atm
Flow rate	16.39	L/min
Inlet temperature	-33.25	°C
Outlet temperature	-32.74	°C

Table 11 Pump results in ASPEN HYSYS
Source: Own Elaboration

Again, the heat exchanger operates countercurrent, on the shell side the coolant is fed by the pump and the pyrolysis gas mixture enters through the tubes. Table 12 lists the results of the simulation of this equipment. It is possible to observe that the outlet temperature of the hot stream is -31.65 °C. This, according to the phase change temperatures shown in Table 4, would favor the formation of condensate in this process stream.

In addition to the above, the temperature profile is illustrated when using the coolant, it is possible to observe the decrease in the temperature of the hot stream, in red, and a slight increase for the cold stream, in blue, along the length of the shell and tube heat exchanger.

It is possible to observe the cooling that the pyrolysis gas mixture undergoes from its feed at 268 °C to its exit from the heat exchanger at -31.65 °C. In addition to the above, the water undergoes a slight heating from its exit from the pump and entrance to the heat exchanger on the shell side, with a temperature of -32.74 °C until it exits at -32.51 °C.

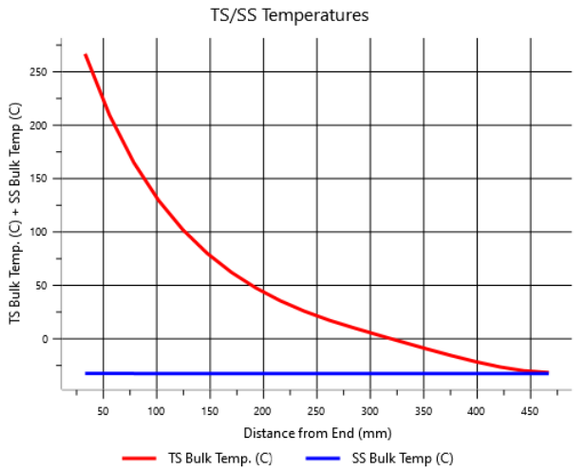

Figure 13 Temperature profile using refrigerant R-717
Source: Own Elaboration

Shell and tube heat exchanger					
		Shell		Tubes	
Process data	Units	Input	Output	Input	Output
Total Flow	$\frac{kg}{h}$		607		1
Steam	$\frac{kg}{h}$	0	0	1	1
Líquid	$\frac{kg}{h}$	607	607	0	0
Temperature	°C	-32.74	-32.51	268	-31.65
Vapor Mass Fraction		0	0	1	1
Pressure	kPa	489.129	489.054	101.325	101.322
Convection coefficient	$\frac{W}{m^2 \cdot K}$		830.1		33.8
Duty	kW				0.1620
Area	m^2				0.2296
UA	$\frac{kJ}{°C \cdot h}$				11.12
LMTD	$°C$				55.22

Table 12 Heat exchanger results using R-717 refrigerant provided by ASPEN HYSYS
Source: Own Elaboration

In addition, there is a slight pressure drop on the hot fluid side, through the heat exchanger tubes, this along the 500 mm of the length of this equipment. Starting with a pressure of 101.325 kPa and exiting at a pressure of 101.322 kPa. This can be observed graphically as shown below:

ISSN: 2410-3462

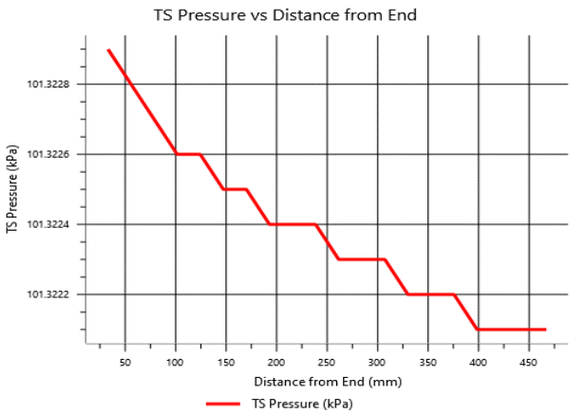

Figure 14 Pressure drop on the pipe side
Source: Own Elaboration

As mentioned above, the film coefficients of both the cold fluid, blue in the graph, and the hot fluid, in red, quantify the influence of fluid, surface and flow properties when convective heat transfer occurs having a value taken from Table 12 of 830.1 and 33.8 W/(m^2· K), respectively.

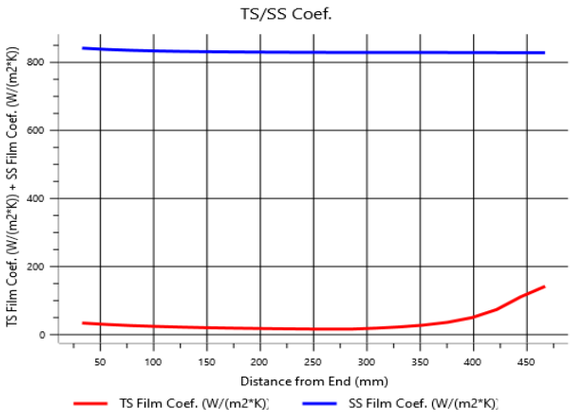

Figure 15 Film coefficients of both fluids
Source: Own Elaboration

On the other hand, to determine the condensate formation, the following graph shows the tube length of 500 mm versus the steam fraction. It is also possible to determine that, at an approximate length of 444 mm there is a decrease in the vapor fraction, i.e., there is condensate formation for this same shell and tube heat exchanger with the use of refrigerant R-717. The above for the composition of the gas mixture taken from the literature and listed in Table 2.

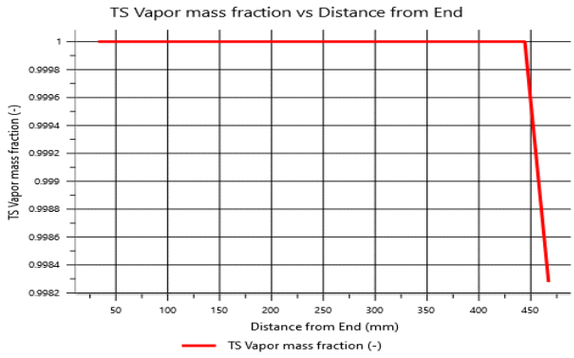

Figure 16 Vapor fraction in the heat exchanger
Source: Own Elaboration

On the other hand, condensate formation is supported by the phase change temperatures of the initial components of the gas phase and presented in Table 4. The following is a list of the components at the exit of the process, for a temperature of -31.65 °C on the tube side, and where the formation of certain pyrolysis gases is favored.

Formula	Vapor phase	Liquid phase
H_2	0.0856	0.0000
CH_4	0.2173	0.0020
CO	0.0482	0.0001
CO_2	0.0621	0.0026
C_2H_4	0.0985	0.0061
C_2H_6	0.0706	0.0077
H_2S	0.0096	0.0015
C_3H_6	0.0695	0.0364
C_4H_8	0.3387	0.9436

Table 13. Molar fractions of the exhaust gas stream with the use of refrigerant R-717
Source: Own Elaboration

2.3 Proposal for the condensation cycle design

On the other hand, a new proposal is made for the design of the condensation cycle where the pump and the heat exchanger of the experimental stage simulated in the previous section using water as cooling liquid are reused.

In this particular case, a cooler and a separator are added to the process, as illustrated in the following process diagram:

ISSN: 2410-3462

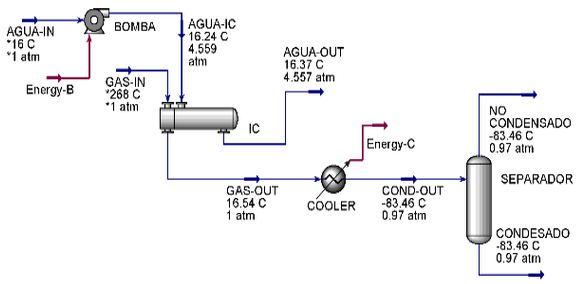

Figure 17 Process diagram for the proposed cooling cycle design
Source: Own Elaboration

Again, the previous conditions of feeding the heat exchanger using water for cooling are resumed. The gases leaving the heat exchanger, which have been cooled to a temperature of 16.54 °C at 1 atm pressure, enter a cooler with the following characteristics:

Cooler		
Parameters	Input	Output
Temperature (°C)	16.54	-83.46
Temperature Delta (°C)		100
Pressure (atm)	1	1
Mass flow (kg/h)	1	1
Duty (kW)		0.1227

Table 14 Cooler specifications
Source: Own Elaboration

The simple cooler is specified through the temperature delta, this specification of a fall of these pyrolysis gases. To observe graphically the condensate formation, a temperature of 100 °C is added to favor the cooling of the gaseous stream and the condensation of the graph corresponding to the vapor fraction as the temperature decreases, i.e., the lower the temperature, the more condensate is obtained.

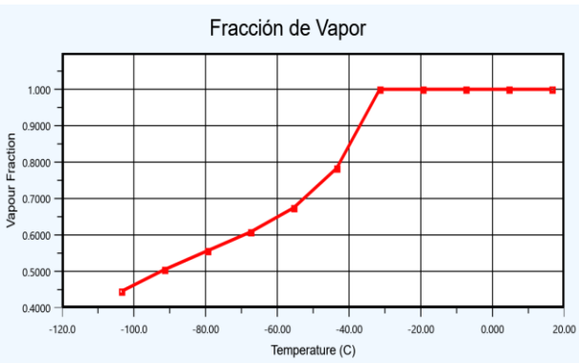

Figure 18 Steam fraction leaving the cooler
Source: Own Elaboration

According to the above, if the vapor fraction graph is observed from left to right, as cooling occurs, the condensation of pyrolysis gases is favored. These results are listed below:

Temperature (°C)	Vapor fraction
16.5428	1.0000
6.5428	1.0000
-3.4571	1.0000
-13.4571	1.0000
-23.4571	1.0000
-33.4571	0.9511
-43.4571	0.7796
-53.4571	0.6861
-63.4571	0.6257
-73.4571	0.5797
-83.4571	0.5379

Table 15 Cooler results
Source: Own Elaboration

The above shows that the use of a cooler favors the phase change and, consequently, the formation of condensate; in addition, it is observed that from a temperature of -33.4571 °C the greatest phase change of the compounds and the formation of liquid phase occurs. Finally, the gases that have condensed the most are listed:

Formula	Vapor phase	Liquid phase
H_2	0.0855	0.0001
CH_4	0.2169	0.0083
CO	0.0481	0.0003
CO_2	0.0620	0.0231
C_2H_4	0.0983	0.0470
C_2H_6	0.0705	0.0585
H_2S	0.0096	0.0105
C_3H_6	0.0694	0.1287
C_4H_8	0.3397	0.7235

Table 16 Molar fractions resulting from condensation with the use of a cooler
Source: Own Elaboration

Finally, the above indicates that at an outlet temperature of -83.46 °C the condensation of gases such as propene and i-butene is favored, with liquid phase mole fractions of 0.1287 and 0.7235, respectively, these gases come from the pyrolytic reactor outlet and compositions taken from the literature as mentioned above.

3. Conclusions

Waste rubber tires have generated a large amount of waste, particularly in Bogota, Colombia. This waste has become an environmental problem due to the agglomerations and the subsequent diseases it can cause.

ISSN: 2410-3462

In this sense, tire pyrolysis is proposed as a viable environmental alternative with a circular economy approach, the products of solid waste pyrolysis can be considered as biofuels with multiple uses. Tests in the experimental stage with scrap rubber tires show that the process works and that the three expected products are obtained and can be separated.

The simulation of the experimental data in the ASPEN HSYSY process simulator allowed corroborating the real operation of the process, taking up compositions from the literature and with operating conditions specific to the experimental stage. In addition, the temperatures of the experimental tests have been compared with those obtained from the simulation, being these similar to those obtained experimentally.

It was found that the use of a refrigerant favors the condensation of pyrolysis gases, allowing a better performance in terms of condensate with a high added value for other processes where its use is required. In addition, if it is desired to use water as cooling liquid, due to its lower utility cost, the use of a cooler is recommended to favor the phase change and the condensation of the gas mixture.

In addition to the above, for further work, it is recommended to perform a gas chromatography of the gas stream leaving the pyrolytic reactor, in order to obtain the precise compositions of the gases and their composition in the gas mixture that enters the heat exchanger for the subsequent condensation stage.

The gases that have not condensed will be re-entered into the pyrolysis reactor as fuels to the burner that feeds energy in the form of heat to the reactor itself. In addition, water that is supplied to the shell and tube heat exchanger as a cooling liquid is recirculated back to the water pump for reuse.

Pyrolysis as an urban solid waste utilization system favors the reduction of tires as waste and provides them with a second use as biofuel or as raw material for other processes, all of this is favorable with the circular economy approach of the project, thus showing a good profitability for the process.

Acknowledge

The authors express their gratitude to the executives of Fundación Universidad de América, the Research Office, and the director of Mechanical Engineering, Eng. María Angélica Acosta, for the support provided to the project with code IIQ-003-2021.

References

[1] L. Cardona Gómez y L. Sánchez-Montoya, “Aprovechamiento de llantas usadas para la fabricación de pisos decorativos”, tesis de grado, Universidad de Medellín, Medellín, Colombia, 2011. [Online]. https://doi.org/CD-ROM 6368 2011

[2] S. E. Castillo-Viveros y M. P. Simancas-Robles, “Estudio de prefactibilidad para la recolección y aprovechamiento de llantas en desuso en la ciudad de Bogotá”, tesis de grado, Universidad Católica de Colombia, Bogotá, Colombia, 2017. [Online]. http://hdl.handle.net/10983/15461.

[3] M. Á. Durán. "Llantas, de enemigo a aliado ambiental". El espectador. https://www.elespectador.com/ciencia/llantas-de-enemigo-a-aliado-ambiental/ (accedido el 22 de noviembre de 2022).

[4] C. Diez, O. Martínez, L. Calvo, J. Cara y A. Morán, “Pirólisis de neumáticos. Influencia de la temperatura final del proceso sobre las emisiones y el poder calorífico de los productos recuperados”. Gestión de residuos. 24 (5), 463–469, 2004.

[5] A. Castellanos, “Propuesta de diseño de un proceso para la generación de energía eléctrica a partir de los residuos de la producción de café”, trabajo de grado, Pontificia Universidad Javeriana, Bogotá, Colombia, 2022. [Online]. https://doi.org/http://hdl.handle.net/10554/7371.

[6] G. Bolívar-Rojas y M. Cuenca-Mayorga, “Evaluación del proceso de pirólisis como alternativa de valorización para la rebaba de caucho en Croydon Colombia S.A.”, trabajo de grado, Fundación Universidad de América, Bogotá, Colombia, 2019. [Online]. http://hdl.handle.net/20.500.11839/7614

[7] P. Basu, “Pyrolysis and Torrefaction. Biomass Gasification Design Handbook”, 65–96, 2010. [Online]. https://doi.org/10.1016/b978-0-12-374988-8.00003-9.

[8] X. Castells-Elías y E. Velo, “Tratamiento y valorización energética de residuos”, trabajo de grado, Fundación Universitaria Iberoamericana, 2012

[9] J. Eiras, F. Segovia, M. Borrachero, J. Monzó, M. Bonilla y J. Payá, “Física y propiedades mecánicas del compuesto de cemento portland espumado que contiene caucho desmenuzado de neumáticos desgastados”. 59, 550–557, 2014. [Online] https://doi.org/10.1016/j.matdes.2014.03.021.

[10] L. Liu, G. Cai, J. Zhang, X. Liu y K., Liu, “Evaluación de propiedades de ingeniería y en Efecto ambiental de la arena/suelo de llantas de desecho recicladas en ingeniería geotécnica: una revisión comprensiva”. Renovar. sust. energia Rev. 126, 09831, 2020. [Online] https://doi.org/10.1016/j.rser.2020.109831.

[11] J. Conesa, A. Fullana y R. Font, “Tire pyrolysis Evolution of volatile and semivolatile compounds. Energy and Fuels": 14, 409-418, 2008.

[12] R. Miranda, C. Segovia y C. Sosa, “Pirólisis de Llantas Usadas: Estudio Cinético e Influencia de Variables de Operación”, Información tecnológica, 17(2), 7-14, 2006. [Online]. https://dx.doi.org/10.4067/S0718-07642006000200003.

[13] H. Teng, A. Serio, A. Wojtowicz, R. Bassilakis y P. Solomon, “Reprocessing of used tires into activated carbon and other productos”. Ind. Eng. Chem. Res., 34, 3102-3111, 1995.
[14] C. Giavarini, “Activate carbon from scrap tyres”, fuel: 64, 1331-1332, 1985.

[15] C. Roy, B. Labrecque y B. Caumia, “Recycling of scrap tires to oil and carbon black by vacuum pyrolysis”, Resource Conservation & Recycling: 4, 203-213, 1990.

[16] A. L. Vera-Hostos, "Estudio experimental del procesamiento de llantas usadas en la producción de biodiésel por medio de transesterificación supercrítica". Ciencia Unisalle.
[Online]. https://ciencia.lasalle.edu.co/cgi/viewcontent.cgi?article=1277&context=ing_ambiental_sanitaria.

[17] D. Acosta, L. Castro, “Diseño del proceso de pirólisis para la producción de biocombustibles a partir de residuos sólidos urbanos”, Proyecto Integral de Grado, Fundación Universidad de América, Bogotá, Colombia, 2021.

Article **Journal Simulation and Laboratory**
June 2022 Vol.9 No.27 31-39

Temperature Profile Estimation in the Core of a Sodium-Cooled Fast Reactor using CFD Modeling

Estimación del Perfil de Temperaturas en el Núcleo de un Reactor Rápido Refrigerado por sodio mediante modelado CFD

DIAZ-ESPINOZA, Gerardo*†, VALLE-HERNANDEZ, Julio and GALLARDO-VILLARREAL, José Manuel

Universidad Politécnica Metropolitana de Hidalgo
Universidad Autónoma del Estado de Hidalgo

ID 1st Author: *Gerardo, Diaz Espinoza* / **ORC ID**: 0000-0003-1293-0275, **CVU CONACYT ID**: 926199

ID 1st Co-author: *Julio, Valle-Hernandez* / **ORC ID**: 0000-0001-8957-0066, **CVU CONACYT ID**: 210743

ID 2nd Co-author: *José Manuel, Gallardo Villarreal* / **ORC ID**: 0000-0002-7578-7229, **CVU CONACYT ID**: 366394

DOI: 10.35429/JSL.2022.26.9.31.39 Received March 30 2022; Accepted June 30, 2022

Abstract

The latest proposal for nuclear systems for application in space are 4th generation reactors that use liquid metals as coolant. The operating conditions, as well as its safety in these matters, is linked to its thermal and fluid dynamic behavior. This paper presents the estimation of the temperature profile of a sodium-cooled fast reactor from the conduction and convection heat transfer mechanisms. The temperature distribution is analyzed in the area of the fuel and the temperature profile of the coolant in the area of the high conductivity pipes. Is established the analysis of nuclear fuel in a one-dimensional, stationary and with power generation. In the GAP area, the analysis is carried out by natural convection, and finally, the cladding in contact with sodium by forced conduction-convection. As results, it is presented the simulation in Computational Fluid Dynamics to determine the temperature profile due to the behavior of the coolant in the pipe when subjected to a constant flow of heat supplied by the nuclear fuel pellets. The temperature profile will allow us to determine the parameters to establish the operating conditions of secondary power conversion systems.

Fluids, Flow, Nuclear Reactor, Heat, Transfer, Analysis

Resumen

La última propuesta de sistemas nucleares para su aplicación en el espacio son los reactores de 4ta generación que utilizan metales líquidos como refrigerante. Las condiciones de operación, así como su seguridad en estos temas está ligado a su comportamiento térmico y fluidodinámico. En este trabajo se presenta la estimación de perfil de temperaturas de un reactor rápido refrigerado por sodio a partir de los mecanismos de transferencia de calor por conducción y convección. La distribución de temperaturas se analiza en la zona del combustible y el perfil de temperatura del refrigerante en la zona de las tuberías de alta conductividad. El análisis del combustible nuclear se establece de manera unidimensional, estacionaria y con generación de energía. En la zona del GAP el análisis se realiza mediante convección natural, finalmente la zona del revestimiento en contacto con el sodio por conducción-convección forzada. Como resultados se presenta la simulación en Dinámica de Fluidos Computacional para determinar el perfil de temperatura debido al comportamiento del refrigerante en la tubería al ser sometida a un flujo constante de calor suministrado por las pastillas de combustible nuclear. El perfil de temperatura nos permitirá determinar los parámetros para establecer las condiciones de operación sistemas secundarios de conversión de potencia.

Fluidos, Flujo, Reactor Nuclear, Heat, Transfer, Analysis

Citation: DIAZ-ESPINOZA, Gerardo, VALLE-HERNANDEZ, Julio and GALLARDO-VILLARREAL, José Manuel. Temperature Profile Estimation in the Core of a Sodium-Cooled Fast Reactor using CFD Modeling. Journal Simulation and Laboratory. 2022, 9-26: 31-39

*Correspondence to Author (e-mail: 213220016@upmh.edu.mx)
†Researcher contributing as first Author.

1. Introduction

The development of new categories of nuclear reactors involves the use of liquid metals as coolant. Unlike thermal reactors that use water as coolant and moderator, fast reactors cooled by liquid metals do not use a moderator (12), because the neutrons generated in the fission process have high energy and move quickly, providing a more efficient system with characteristics to withstand high operating temperatures.

The heating and cooling of fluids inside high conductivity pipes are recurrent heat transfer processes in nuclear systems, being the heating of the coolant by extracting heat from the fuel pellets and the cooling of the coolant by circulating throughout the system, this process allows transferring heat to another area of the system where it is required; the latter establishes the parameterization of subsequent components either heat exchangers or power converters.

This configuration allows to define the nuclear system that we will analyze in this article, being the Lunar Evolutionary Growth Optimized (LEGO) Nuclear Reactor the one implemented to supply electric power for possible lunar settlements. As characteristics it presents Uranium Dioxide (UO2) as nuclear fuel stored in 84 pellets, contained in a helium gap and SS-316 stainless steel cladding, 43 high conductivity pipes and cooled by sodium, delivering a thermal power of 24 kWt.

Therefore, observing the behavior of the coolant in this type of nuclear reactors will be the main objective of this article, the characteristics of the transport of liquid metal as coolant through the high conductivity pipes of the reactor system will be taken into consideration and a heat transfer analysis will be performed by CFD modeling that will allow obtaining temperature profiles in certain cross sections of the pipe, giving guideline to observe the final temperature at the outlet of the same.

2. Methodology

The methodology developed in this work is presented below:

- Description of the Lunar Nuclear Reactor
- Mathematical foundation for system analysis.
- Heat Transfer Model
- Initial Coolant Parameters at the Inlet of High Conductivity Pipelines.
- System Modeling in Computational Fluid Dynamics
- Estimation of the temperature transferred from the nuclear reactor to the coolant.

3. Description of the Lunar Nuclear Reactor

The Lunar Evolutionary Growth Optimized (LEGO) Reactor contains stainless steel clad UO2 fuel pellets that are structurally and thermally bonded to high conductivity pipes carrying sodium. Heat is conducted from the fuel pellets to the pipes, which then carry the heat to a power conversion system (1).

It is a type of Clustered Lunar Regolith Reactor and called Advanced Generation 4 because it is a liquid metal-cooled Fast Reactor composed of six subcritical nuclear reactor subunits capable of generating up to 24 kWt each. A fundamental group composed of six subunits provides 30 kWe to a lunar base.

3.1. Reactor Core Geometry

The LEGO reactor uses the existing lunar regolith as a radiation shielding material and neutron reflector. Each subunit is embedded in the lunar surface to create a neutron-coupled reactor assembly capable of reaching criticality to generate power. The reactor subunits have a subcritical design, which promotes safety in the event of a launch accident (1).

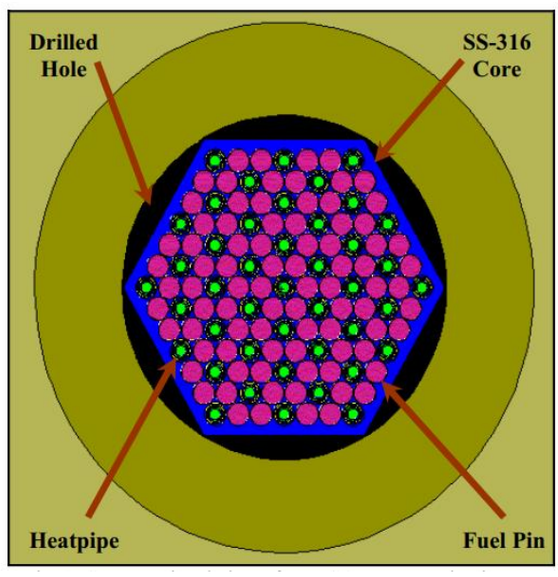

Figure 1 Top (1) and Isometric view of the core of a LEGO Reactor subunit

ISSN: 2410-3462

Fast fission reactor systems are capable of fissioning any additional actinides produced in the fuel and can achieve deeper burnup levels than conventional thermal reactors. The lower operating power per subunit reduces neutron damage and thermal loads compared with larger reactor systems, which increases the longevity of the intrinsic properties of the reactor materials (1).

3.2. Characteristics of the Fuel Assemblies

It is composed of enriched Uranium Dioxide (UO2), and for the system lining of austenitic stainless steel (SS-316) containing molybdenum, being more resistant to corrosion offering higher creep, stress to rupture and tensile strength at elevated temperatures (16).

This hexagonal packing configuration allows a high heat transfer ratio and is designed to deliver 24 kWt to the power conversion system. The core has 84 fuel rods and 43 high-conductivity pipes that carry the metallic liquid (sodium) (1).

The fuel rods have a diameter of 1.6160 cm contained in 1.6414 cm (SS-316) tubing with helium-filled spaces. The high conductivity pipes are modeled with a 1.1254 cm SS-316 casing with a 0.7878 cm SS-316 wick and 0.0844 cm thickness (1).

The fuel is 93% enriched in 235U at 95% of theoretical density. The fuel rods are 49 cm long with a total core height of 54 cm; high conductivity tubing extends an additional 106 cm above the core. The SS-316 monolithic hexagonal core design has a circumscribed corner-to-corner diameter of 23.80 cm.

A tapered stainless steel base extends 9 cm below the core to provide support, stability and alignment within the drilled hole (1).

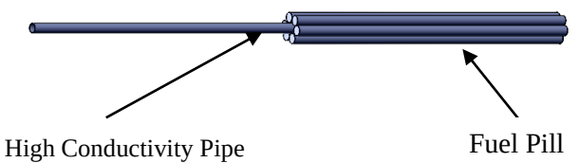

Figure 2 Side view of the core of a LEGO Reactor subunit section

Parameters	
Fuel Pad Diameter (m)	0.016414
High Conductivity Pipe Diameter (m)	0.011254
Coating Thickness (m)	0.000844
High Conductivity Pipe Length (m)	1.06
Length Fuel Pads (m)	0.49

Table 1 Geometric Parameters of the Model (1)

3.3. Coating

For the SS-316 stainless steel alloy used on the surface of high conductivity pipes, the addition of austenitic chromium-nickel with molybdenum increases corrosion resistance and improves pitting resistance to chloride ion solutions and provides higher resistance to elevated temperatures (17).

3.4. Reactor Coolant

Due to the large amount of energy released by the core, a working fluid with good heat transfer characteristics is used. The LEGO reactor, being a fast reactor, uses a liquid metal-based coolant system, being sodium the one assigned to extract the emitted heat and having as an advantage that it can remain in liquid state in a high temperature range (1).

To keep the sodium as a suitable candidate, it is established that, compared with other refrigerants used in terrestrial counterparts, sodium has a low need for pumping power, can be used at atmospheric pressure, works well below the boiling point which makes possible its ability to absorb considerable energy in emergency conditions (3).

Likewise, it is a fluid with a tendency to dissolve penetrating fission products due to some failure, as well as to retain them.

4. Mathematical Foundation for System Analysis

The simulation of the phenomena corresponding to fluid-dynamic perturbations in systems represents the response of fluids to mechanical forces, motion and heat transfer. To observe this behavior, the conservation of energy, conservation of momentum and conservation of mass equations are defined. (2).

ISSN: 2410-3462

4.1. Conservation of mass

The mass balance through the control volume is expressed by the continuity equation:

$$\frac{\partial \rho}{\partial t} + \nabla \cdot (\rho \vec{v}) = 0 \quad (1)$$

where ρ is the density of the fluid, i.e. the mass per unit volume, v ⃗ is the velocity field and t the time variable.

4.2. Conservation of Momentum

Since the external forces acting on a control volume are represented by the ratio of change with respect to time of the linear momentum and the flow over a surface is expressed by:

$$\rho \frac{\partial \vec{v}}{\partial t} + \rho(\vec{v} \cdot \nabla)\vec{v} = -\nabla \mathrm{p} + \rho \vec{g} + \nabla \cdot \tau_{ij} \quad (2)$$

where g ⃗ the acceleration of gravity, τ_ij, the viscous stress tensor;

4.3 Energy Conservation

$$\rho \frac{\partial E}{\partial t} + \rho \nabla \cdot (\vec{v} E) = \nabla \cdot (k \nabla \mathrm{T}) + \rho \vec{g} + \nabla \cdot (\sigma \cdot \vec{v}) + W_f \dot{+} \dot{q}_H \quad (3)$$

where E is the fluid energy, T the temperature, k the thermal conductivity, g ⃗ the acceleration of gravity, σ the stress tensor; W_f the work done on the fluid and (q ̇_H) ̇ the heat supplied to the fluid.

However, there are phenomena that introduce additional nonlinearities, such as turbulence or chemical reactions.

This makes it impossible to obtain an analytical solution, making it necessary to resort to approximate methods, such as numerical techniques, for its solution. (18).

5. Heat Transfer Model

5.1. Heat Transfer in the Fuel Cell

It is important to know the temperature distribution in the system, so it is considered to perform the analysis in cylindrical coordinates as follows:

$$\frac{1}{r}\frac{\partial}{\partial r}\left(kr\frac{\partial T}{\partial r}\right) + \frac{1}{r^2}\frac{\partial}{\partial \phi}\left(kr\frac{\partial T}{\partial r}\right) + \frac{\partial}{\partial z}\left(k\frac{\partial T}{\partial r}\right) + \dot{e_{gen}} = \rho c \frac{\partial T}{\partial t} \quad (4)$$

For this article, the centerline is taken as the origin of the r-coordinate. Due to the symmetry in the z-direction and the azimuthal direction, we can separate the variables and simplify the problem in a one-dimensional way, as well as:

1. Heat conduction in the axial direction is negligible with respect to heat conduction in the radial direction.
2. Heat generation in the fuel is uniform at each of the radial nodes.
3. The heat transfer is considered stationary for the system.
4. No heat generation in the coating.

Thus the above equation simplifies to:

$$\frac{1}{r}\frac{\partial}{\partial r}\left(kr\frac{\partial T}{\partial r}\right) + \frac{q_v}{k} = 0 \quad (5)$$

5.2. Heat Transfer at the GAP

Natural Convection

For a system of concentric cylinders the natural convection heat transfer rate is expressed as:

$$\dot{Q} = \frac{2\pi k_{eff}}{\ln\left(\frac{D_o}{D_i}\right)}(T_i - T_o) \quad (6)$$

where k_eff is the effective thermal conductivity, i.e., for convective heat transfer in a closed room it is analogous to conduction whenever it is replaced as $k_{eff} = kNu$.

For the analysis of the Nusselt number in natural convection, the heat transfer relationships based on experimental studies are taken, which determines that:

$$Nu = \frac{hLc}{k} = C(Gr_L P_r) = CRa_L \quad (7)$$

Where 〖Ra〗 _L is the Rayleigh number, which is the product of the Grashof and Prandtl numbers; which describes the relationship between buoyancy and viscosity within the fluid, and the Prandtl number, which describes the relationship between the diffusivity of the quantity of motion and the thermal diffusivity; therefore, it will be obtained that

$$\mathrm{Ra_L} = \mathrm{Gr_L P_r} = \frac{g\beta(T_s - T_\infty)Lc^3}{v^2}\mathrm{Pr} = \frac{g\beta(T_s - T_\infty)Lc^3}{v\infty} \quad (8)$$

Being g the gravity, β the coefficient of volumetric expansion, Ts the surface temperature, T∞ the temperature of the fluid far enough from the surface, Lc the characteristic length of the geometric configuration and v the kinematic viscosity of the fluid.

For steady flow heat at the surface, the ratio is known to be Q ̇=q_s A_s, not knowing the surface temperature, it is related to the uniform flow characteristics which allows relating the Rayleigh interval to the Nusselt number for certain geometric configuration, as shown in the following equation.:

$$\mathrm{Nu} = \left\{ 0.825 + \frac{0.387\mathrm{Ra_L}^{\frac{1}{6}}}{\left[1+\left(\frac{0.492}{\mathrm{P_R}}\right)^{\frac{9}{16}}\right]^{\frac{8}{27}}} \right\}^2 \quad (9)$$

The correlation of heat transfer by natural convection in the subchannel in the developing region for a constant heat flux can be formulated as follows:

$$\mathrm{Nu} = \mathrm{C(Gr_L P_r)} \quad (10)$$

5.3.Heat Transfer in Coatings

– Coolant

Forced Internal Convection

This last section of the heat transfer mechanisms presents the forced convection as part of the mathematical model to be verified by numerical simulation, this because the coolant was forced through the pipes this mechanism establishes the extraction of heat from the reactor, so it is defined as follows:

If the heat transfer coefficient is known for a given geometry and specific flow conditions, the rate of heat transfer at the prevailing temperature difference can be calculated using Equation 11

$$q_c = h_c A(Ts - T\infty) \quad (11)$$

Where q_c is the heat flux, h_c is the convective heat transfer coefficient, Ts is the surface temperature and T∞ is the fluid temperature. For the analysis of heat transfer by forced convection, the following correlation is presented, which allows observing the behavior of the fluid flow involving the thermal conductivity, the specific heat and the type of flow it has:

$$Nu = (ReP_r) \quad (12)$$

Where:

$$Nu = Número\ de\ Nusselt = \frac{hD}{k}$$
$$Re = Número\ de\ Reynolds = \frac{\rho VD}{\mu}$$
$$Pr = Número\ de\ Prandtl = \frac{C_p\mu}{k}$$

Likewise, the Dittus-Boelter correlation is implemented for heated fluid and turbulent flow to calculate the Nusselt flow number in a circular pipe based on equation 12.

$$Nu = 0.023Re^{0.8}P_r^{0.4} \quad (13)$$

Finally, by relating equations 12 and 14, the value of the convective heat transfer coefficient is determined, obtaining:

$$h = \frac{Nuk}{Dh} \quad (14)$$

where Dh is the hydraulic diameter where it involves the Area and Perimeter of the pipeline.

6. Initial Parameters for Numerical Modeling

The properties of the coolant are represented due to its behavior in certain temperature ranges, for this article the interpolation polynomials were generated referring to that variation that may exist throughout the flow section.

Following are the properties that were determined by the interpolation function:

Thermal Conductivity $\left(\frac{W}{mK}\right)$

$$k = 91.8 - (49 * 10^{-3})T + (3.469 * 10^{-18})T^2 - (3.881 * 10^{-21})T^3 + (1.6544 * 10^{-24})T^4 \quad (15)$$

ISSN: 2410-3462

Specific Heat $\left(\frac{J}{kg\,°C}\right)$

$$Cp = 1435.9 - (0.5700643)T + (0.0004275833)T^2 + (0.0000000439286)T^3 - (19.04 * 10^{-12})T^4 \quad (16)$$

Dynamic Viscosity $\left(\frac{Pa}{s}\right)$

$$\mu = 0.0011017 - 0.0000054859T + (1.43913 * 10^{-8})T^2 - (1.76067 * 10^{-11})T^3 + (87.8667 * 10^{-15})T^4 \quad (17)$$

Density $\left(\frac{kg}{m^3}\right)$

$$\rho = 949.93 - (226.6 * 10^{-3})T - (2.61667 * 10^{-5})T^2 + (2.25 * 10^{-8})T^3 - (8.3333 * 10^{-12})T^4 \quad (18)$$

The LEGO reactor is designed for a high thermal power range, so the thermal behavior of the walls of the system is bounded by the characteristics of the coating material, for the case of the walls of the pipes high conductivity temperature limit is 1250 K (977 ° C).

For the coating implemented in the pipes, we will assign the values that are thermal conductivity, specific heat and density for stainless steel that will provide an approximation of the behavior of the wall with the flow of the coolant to provide a constant flow of heat.

Parameters	
Thermal Conductivity $\left(\frac{W}{mK}\right)$	16.2
Specific Heat $\left(\frac{J}{kgK}\right)$	502.48
Density $\left(\frac{kg}{m^3}\right)$	8030

Table 2 Coating Parameters

The following considerations will be taken into account to carry out the CFD modeling, initially it is taken as an internal flow, because it will be confined in a pipe, it is established to work with a turbulent flow.

An analysis of forced internal convection will be handled since the coolant will be forced to flow through the high conductivity pipe involving stationary conditions, i.e., the fluid properties will not change with respect to time, only with respect to temperature.

Finally, it will take into account a one-dimensional analysis, the fluid properties will vary in one direction only.

Parameters	
Speed $\left(\frac{m}{s}\right)$	5.02
Fluid inlet temperature $(°C)$	800
Heat Flow $\left(\frac{MW}{m^2}\right)$	1.64

Table 3 Wall Parameters

To obtain the temperature profiles, the position of the coolant flow is presented as longitudinal through the high conductivity pipe, the temperature values were obtained due to the constant flow of heat in the wall of the entire section.

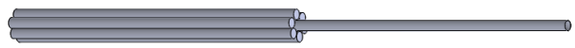

Figure 3 Side View of Coolant Flow in Position to CFD Modeling

7. Results

7.1. Temperature Distribution - Fuel

Next, the results obtained from the analytical calculation obtained due to the heat transfer mechanisms by conduction Eq. (5) and convection Eq. (11) in the fuel zone, the GAP and the cladding as a function of the thermal power of the fuel and the coolant flow are presented.

In Figure 4, the heat transfer by conduction is implemented in a one-dimensional and stationary way, due to these considerations the heat transfer equation by conduction in cylindrical coordinates is simplified, allowing to observe the behavior of the temperature in a radial way.

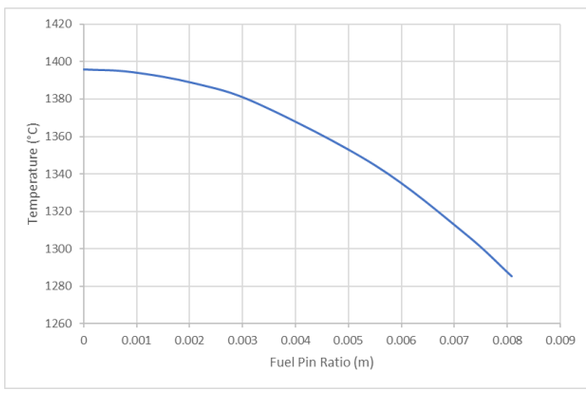

Figure 4 Temperature Distribution - Fuel Cylinder

Using the boundary conditions at T (0) and T(r), the equation was obtained to determine the temperature at each radial node generating the temperature distribution up to the outer wall of the fuel pellet GAP is found.

7.2.Temperature Distribution - GAP

The fission gases are released to the free volume of the rod, which increases the internal pressure causing the nuclear fuel to swell, this zone is filled with helium so the heat transfer in this section will be analyzed by natural convection, it has been taken into account a series of dimensionless numbers that allow observing the behavior when subjected to the thermal power of the fuel.

The parameterization of this zone was carried out by means of the Nusselt number, which correlates to the Rayleigh number and the Prandtl number Eq. (7). Taking into account the gravity of the moon simulating a mission in that site, the value will be taken as g=1.62 m/s^2, likewise the kinematic viscosity of helium being v= 0.000158359 m^2/s, based on Eq. (8) we can obtain the Grashof number. Subsequently, the Prandtl number relating the dynamic viscosity and thermal conductivity can be correlated with the Grashof number to determine the Rayleigh number.

Being the Rayleigh number a guideline to determine the Nusselt number which, establishing the variation of the same in each value of the radius in the thickness of the GAP, the temperature distribution is determined as shown in the following figure.

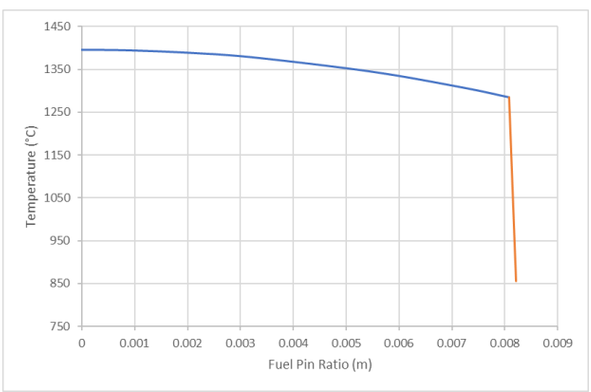

Figure 5 Fuel Temperature Distribution – GAP

Finally, the properties of sodium are presented by means of the interpolation polynomials (Equation 15-18) that are affected by the temperature changes to which it will be subjected. The value of the mass flow is proposed which, based on the area of the pipe and the density of the fluid, the velocity at which it will flow in that cross section can be obtained, thus obtaining $v = 6.85 \frac{m}{s}$

Having the speed and properties of the coolant at an average temperature, we proceed to apply Eq. (12) to determine the Prandtl and Reynolds number, the Dittus - Boelter correlation marks the starting point to implement the above dimensionless numbers, obtaining the value of the Nusselt number of 46.12. By means of equation 14, the convective heat transfer coefficient is obtained being h=202 kW/(m^2 C) which allowed based on equation 11 to obtain the wall temperature due to the temperature at the proposed outlet, this temperature assumption, was obtained by varying values to achieve the thermal power of the reactor.

By the above variation, the temperature of the wall that will be in contact with the coolant was obtained, which will not allow to obtain the heat loss due to the internal wall temperature of the liner and the new temperature taking into account that a △T=429 °C was determined. Based on this value, the heat loss in the entire liner section was determined.

7.3. Temperature Distribution - Coating

Finally, implementing the conduction heat conduction equation in cylindrical coordinates, the temperature distribution is determined by knowing the heat loss in the coating, obtaining Figure 6 according to the changes related to the GAP and its temperature distribution.

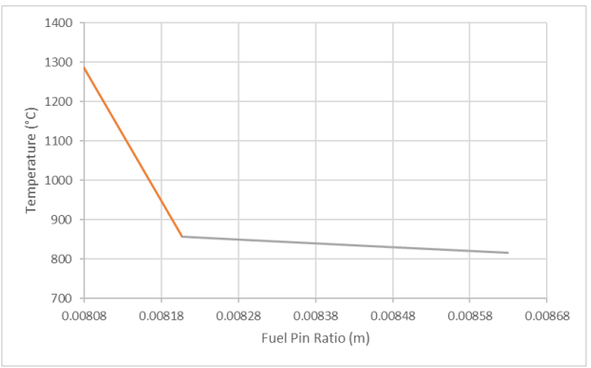

Figure 6 GAP Temperature Distribution – Coating

ISSN: 2410-3462

The ΔTs for each section and the final temperatures at each boundary are presented below.

ΔFuel	110 °C
ΔGAP	429°C
ΔClad	43 °C
Tin - Fuel	1396 °C
Text - Fuel	1285 °C
Text - GAP	856 °C
Text - Revestimiento	812 °C

The initial parameters of the CFD modeling will be some of the values obtained analytically being the constant heat flux, the coolant inlet temperature and velocity. As a means of verification, the use of CFD techniques was implemented where the geometry of the high conductivity pipe was generated taking the diameter and length.

Likewise, the boundary conditions and the parameterization of the inlet, outlet and walls were generated obtaining the temperature profile and contour.

7.4.Temperature Profiles - Pumping Pipelines

Figure 7 shows the streamlines of the temperature change in the fluid due to a constant heat flow in the wall area, this value was obtained due to the thermal power of the fuel pellet.

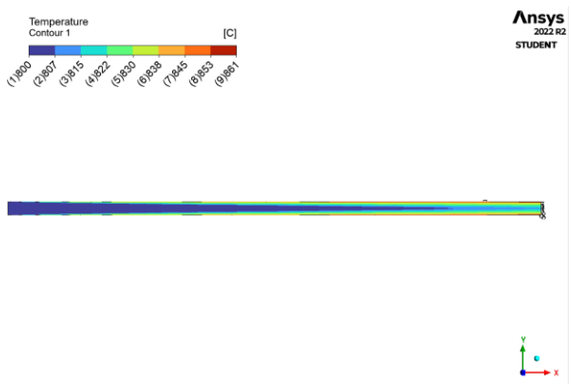

Figure 7 Power Lines – Pipelines

You can observe the temperature increase as the position of the coolant changes through the longitudinal section, in the same way the temperature at the inlet and outlet of the system will be taken as a reference, observing the temperature distribution in the coolant flow.

It could also observe the behavior of the thermal boundary layer along the entire section, mainly analyzes the thermal input region where it begins to increase the fluid temperature, to reach a point where the temperature will remain constant so it reaches the region fully developed thermally being this the area of interest for this article due to the temperature at the outlet of the pipe.

Finally, in Figure 8 you can see the temperature profile of the coolant flow to be subjected to a constant flow of heat observing the temperature distribution from the inlet temperature to the outlet temperature, this because it was determined the temperature at the wall.

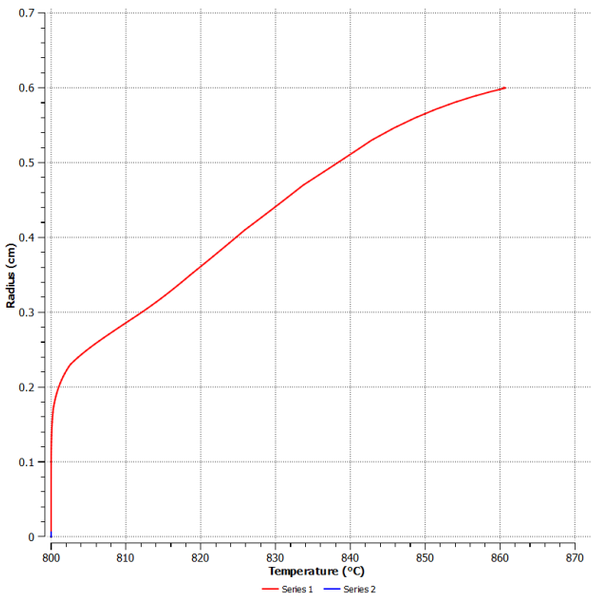

Figure 8 Coolant Flow Temperature Profiles as a function of radius

	Analytical	CFD
Tint - Revestimiento	856 °C	861 °C
Text - Revestimiento	815 °C	825 °C
Tout - Refrigerante	814 ° C	819 °C

8. Conclusions

Based on the results obtained, the following conclusions will be presented:

– Increased heat transport due to forced coolant flow will cause a decrease in reactor temperature.
– The behavior of the temperature distribution in the reactor-coolant zone having appropriate ΔT with respect to the thermal power delivered by the nuclear reactor was observed.

ISSN: 2410-3462

- The results obtained due to the temperature distribution in the reactor area and the coolant flow will keep the coolant in liquid state, causing a redesign of the LEGO Reactor, giving guidelines for future work regarding the implementation of a pumping system that drives the coolant to the potassium boiler.
- It was observed that the temperature at the output in the CFD modeling approached with a difference of 0.8% to the analytical modeling performed.

9. Funding

This work has been funded by CONACYT Grant Number 926199.

References

[1] Bess, John Darrell. (2008) A Basic LEGO Reactor Design for the Provision of Lunar Surface Power. United States. (INL/CON--08-14353).

[2] Cengel, Yunus A. (2004) Transferencia De Calor Y Masa. Fundamentos y aplicaciones. University of Nevada, Reno.

[3] Jeltsov, Marti. (2018) Validation and Application of CFD to Safety-Related Phenomena in Lead-Cooled Fast Reactors. KTH Royal Institute of Technology. Pag 15-18.

[4] Toapanta, Ramos. Luis F. (2019) Estudio Numerico y Comparativo del Efecto de Turbulencia en Codos y Dobleces para Distribución de Agua Sanitaria. Pag 8-11.

[5] Crevillén, García. David (2012) Simulación Numérica del Flujo a través del Tubo Difusor de una Turbina de Reacción. Factores de Mejora de su Eficiencia. Universidad Politécnica de Cartagena.

[6] Scarpin, Gustavo (2012) Modelo Adiabático Ideal de Motores Stirling. Proyecto, Instituto Universitario Aeronáutico. DMA-003/12.

[7] Koshkin N. I., Shirkévich M. G.. Manual de Física elemental, Edt. Mir (1975) págs. 74-75.

[8] Park, Ye Young (2019) Design Study of Heat Pipes for Nuclear Spaceship Applications. Department of Nuclear Engineering, Ulsan National Institute of Science and Technology (UNIST), 50 UNIST-gil, Ulju-gun, Ulsan, 44919, Republic of Korea.

[9] Sleicher, C.A., & Rouse, M.W. (1975). A convenient correlation for heat transfer to constant and variable property fluids in turbulent pipe flow. International Journal of Heat and Mass Transfer, 18, 677-683.

[10] Palos Mario, *et al* (2019) Lunar ISRU Energy Storage And Electricity Generation, European Space Agency.

[11] L. Mason, D. Poston, and L. Qualls. System Concepts for Affordable Fission Surface Power. Space Technology and Applications International Forum (STAIF), 2008.

[12] INTERNATIONAL ATOMIC ENERGY AGENCY, Status of Fast Reactor Research and Technology Development, IAEA-TECDOC-1691, IAEA, Vienna (2013)

[13] KAZACHKOVSKIY, O D *et al* , "The present status of the fast reactor programme in the USSR" (Proc. Int Conf on Nuclear Power and its Fuel Cycle, Salzburg, 1977) 1, Paper IAEA-CN-36/356, IAEA, Vienna (1977) 393-414

[14] Khodarev, Eduard (1978) Liquid Metal Fast Breeder Reactors. International Atomic Energy Agency, Bulletin 20 (6), 29.38

[15] Judd, W.C. *et al* (1964) Analysis Of Essential Nuclear Reactor Materials. New Brunswick Lab., AEC, NJ (United States)

[16] Lister, Derek H. (2014) Nuclear Plant Materials and Corrosion. University of New Brunswick.

[17] Combined Metals of Chicago (2017) Alloy 316L Stainless Steel. Bellwood Service Center. IL. USA.

[18] Vicente, S. Pablo (2016) Análisis Termohidráulico de la Refrigeración del Combustible Nuclear mediante Dinámica de Fluidos Computacional. Universidad Politécnica de Madrid. Master en Ingeniería Industrial.

ISSN: 2410-3462

[Title in Times New Roman and Bold No. 14 in English and Spanish]

Surname (IN UPPERCASE), Name 1st Author†*, Surname (IN UPPERCASE), Name 1st Coauthor, Surname (IN UPPERCASE), Name 2nd Coauthor and Surname (IN UPPERCASE), Name 3rd Coauthor

Institutional Affiliation of Author including Dependency (No.10 Times New Roman and Italic)

International Identification of Science - Technology and Innovation

ID 1st Author: (ORC ID - Researcher ID Thomson, arXiv Author ID - PubMed Author ID - Open ID) and CVU 1st author: (Scholar-PNPC or SNI-CONACYT) (No.10 Times New Roman)

ID 1st Coauthor: (ORC ID - Researcher ID Thomson, arXiv Author ID - PubMed Author ID - Open ID) and CVU 1st coauthor: (Scholar or SNI) (No.10 Times New Roman)

ID 2nd Coauthor: (ORC ID - Researcher ID Thomson, arXiv Author ID - PubMed Author ID - Open ID) and CVU 2nd coauthor: (Scholar or SNI) (No.10 Times New Roman)

ID 3rd Coauthor: (ORC ID - Researcher ID Thomson, arXiv Author ID - PubMed Author ID - Open ID) and CVU 3rd coauthor: (Scholar or SNI) (No.10 Times New Roman)

(Report Submission Date: Month, Day, and Year); Accepted (Insert date of Acceptance: Use Only ECORFAN)

Abstract (In English, 150-200 words)

Objectives
Methodology
Contribution

Abstract (In Spanish, 150-200 words)

Objectives
Methodology
Contribution

Keywords (In English)

Indicate 3 keywords in Times New Roman and Bold No. 10

Keywords (In Spanish)

Indicate 3 keywords in Times New Roman and Bold No. 10

Citation: Surname (IN UPPERCASE), Name 1st Author, Surname (IN UPPERCASE), Name 1st Coauthor, Surname (IN UPPERCASE), Name 2nd Coauthor and Surname (IN UPPERCASE), Name 3rd Coauthor. Paper Title. Journal Simulation and Laboratory. Year 1-1: 1-11 [Times New Roman No.10]

* Correspondence to Author (example@example.org)
† Researcher contributing as first author.

Introduction

Text in Times New Roman No.12, single space.

General explanation of the subject and explain why it is important.

What is your added value with respect to other techniques?

Clearly focus each of its features

Clearly explain the problem to be solved and the central hypothesis.

Explanation of sections Article.

Development of headings and subheadings of the article with subsequent numbers

[Title No.12 in Times New Roman, single spaced and bold]

Products in development No.12 Times New Roman, single spaced.

Including graphs, figures and tables-Editable

In the article content any graphic, table and figure should be editable formats that can change size, type and number of letter, for the purposes of edition, these must be high quality, not pixelated and should be noticeable even reducing image scale.

[Indicating the title at the bottom with No.10 and Times New Roman Bold]

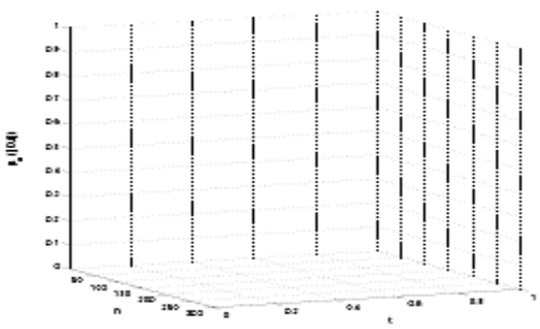

Graphic 1 Title and *Source (in italics)*

Should not be images-everything must be editable.

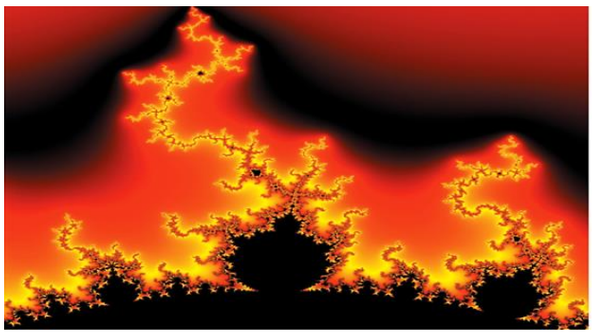

Figure 1 Title and *Source (in italics)*

Should not be images-everything must be editable.

Table 1 Title and *Source (in italics)*

Should not be images-everything must be editable.

Each article shall present separately in **3 folders**: a) Figures, b) Charts and c) Tables in .JPG format, indicating the number and sequential Bold Title.

For the use of equations, noted as follows:

$$Y_{ij} = \alpha + \sum_{h=1}^{r} \beta_h X_{hij} + u_j + e_{ij} \qquad (1)$$

Must be editable and number aligned on the right side.

Methodology

Develop give the meaning of the variables in linear writing and important is the comparison of the used criteria.

Results

The results shall be by section of the article.

Annexes

Tables and adequate sources

Thanks

Indicate if they were financed by any institution, University or company.

ISSN 2410-3462

Conclusions

Explain clearly the results and possibilities of improvement.

References

Use APA system. Should not be numbered, nor with bullets, however if necessary numbering will be because reference or mention is made somewhere in the Article.

Use Roman Alphabet, all references you have used must be in the Roman Alphabet, even if you have quoted an Article, book in any of the official languages of the United Nations (English, French, German, Chinese, Russian, Portuguese, Italian, Spanish, Arabic), you must write the reference in Roman script and not in any of the official languages.

Technical Specifications

Each article must submit your dates into a Word document (.docx):

Journal Name
Article title
Abstract
Keywords
Article sections, for example:

1. Introduction
2. Description of the method
3. Analysis from the regression demand curve
4. Results
5. Thanks
6. Conclusions
7. References

Author Name (s)
Email Correspondence to Author
References

Intellectual Property Requirements for editing:

-Authentic Signature in Color of Originality Format Author and Coauthors

-Authentic Signature in Color of the Acceptance Format of Author and Coauthors

-Authentic Signature in Color of the Conflict of Interest Format of Author and Co-authors

ISSN 2410-3462

Reservation to Editorial Policy

Journal Simulation and Laboratory reserves the right to make editorial changes required to adapt the Articles to the Editorial Policy of the Research Journal. Once the Article is accepted in its final version, the Research Journal will send the author the proofs for review. ECORFAN® will only accept the correction of errata and errors or omissions arising from the editing process of the Research Journal, reserving in full the copyrights and content dissemination. No deletions, substitutions or additions that alter the formation of the Article will be accepted.

Code of Ethics - Good Practices and Declaration of Solution to Editorial Conflicts

Declaration of Originality and unpublished character of the Article, of Authors, on the obtaining of data and interpretation of results, Acknowledgments, Conflict of interests, Assignment of rights and Distribution

The ECORFAN-Mexico, S.C Management claims to Authors of Articles that its content must be original, unpublished and of Scientific, Technological and Innovation content to be submitted for evaluation.

The Authors signing the Article must be the same that have contributed to its conception, realization and development, as well as obtaining the data, interpreting the results, drafting and reviewing it. The Corresponding Author of the proposed Article will request the form that follows.

Article title:

- The sending of an Article to Journal Simulation and Laboratory emanates the commitment of the author not to submit it simultaneously to the consideration of other series publications for it must complement the Format of Originality for its Article, unless it is rejected by the Arbitration Committee, it may be withdrawn.

- None of the data presented in this article has been plagiarized or invented. The original data are clearly distinguished from those already published. And it is known of the test in PLAGSCAN if a level of plagiarism is detected Positive will not proceed to arbitrate.

- References are cited on which the information contained in the Article is based, as well as theories and data from other previously published Articles.

- The authors sign the Format of Authorization for their Article to be disseminated by means that ECORFAN-Mexico, S.C. In its Holding Bolivia considers pertinent for disclosure and diffusion of its Article its Rights of Work.

- Consent has been obtained from those who have contributed unpublished data obtained through verbal or written communication, and such communication and Authorship are adequately identified.

- The Author and Co-Authors who sign this work have participated in its planning, design and execution, as well as in the interpretation of the results. They also critically reviewed the paper, approved its final version and agreed with its publication.

- No signature responsible for the work has been omitted and the criteria of Scientific Authorization are satisfied.

- The results of this Article have been interpreted objectively. Any results contrary to the point of view of those who sign are exposed and discussed in the Article.

Copyright and Access

The publication of this Article supposes the transfer of the copyright to ECORFAN-Mexico, SC in its Holding Bolivia for it Journal Simulation and Laboratory, which reserves the right to distribute on the Web the published version of the Article and the making available of the Article in This format supposes for its Authors the fulfilment of what is established in the Law of Science and Technology of the United Mexican States, regarding the obligation to allow access to the results of Scientific Research.

Article Title:

Name and Surnames of the Contact Author and the Coauthors	Signature
1.	
2.	
3.	
4.	

Principles of Ethics and Declaration of Solution to Editorial Conflicts

Editor Responsibilities

The Publisher undertakes to guarantee the confidentiality of the evaluation process, it may not disclose to the Arbitrators the identity of the Authors, nor may it reveal the identity of the Arbitrators at any time.

The Editor assumes the responsibility to properly inform the Author of the stage of the editorial process in which the text is sent, as well as the resolutions of Double-Blind Review.

The Editor should evaluate manuscripts and their intellectual content without distinction of race, gender, sexual orientation, religious beliefs, ethnicity, nationality, or the political philosophy of the Authors.

The Editor and his editing team of ECORFAN® Holdings will not disclose any information about Articles submitted to anyone other than the corresponding Author.

The Editor should make fair and impartial decisions and ensure a fair Double-Blind Review.

Responsibilities of the Editorial Board

The description of the peer review processes is made known by the Editorial Board in order that the Authors know what the evaluation criteria are and will always be willing to justify any controversy in the evaluation process. In case of Plagiarism Detection to the Article the Committee notifies the Authors for Violation to the Right of Scientific, Technological and Innovation Authorization.

Responsibilities of the Arbitration Committee

The Arbitrators undertake to notify about any unethical conduct by the Authors and to indicate all the information that may be reason to reject the publication of the Articles. In addition, they must undertake to keep confidential information related to the Articles they evaluate.

Any manuscript received for your arbitration must be treated as confidential, should not be displayed or discussed with other experts, except with the permission of the Editor.

The Arbitrators must be conducted objectively, any personal criticism of the Author is inappropriate.

The Arbitrators must express their points of view with clarity and with valid arguments that contribute to the Scientific, Technological and Innovation of the Author.

The Arbitrators should not evaluate manuscripts in which they have conflicts of interest and have been notified to the Editor before submitting the Article for Double-Blind Review.

Responsibilities of the Authors

Authors must guarantee that their articles are the product of their original work and that the data has been obtained ethically.

Authors must ensure that they have not been previously published or that they are not considered in another serial publication.

Authors must strictly follow the rules for the publication of Defined Articles by the Editorial Board.

The authors have requested that the text in all its forms be an unethical editorial behavior and is unacceptable, consequently, any manuscript that incurs in plagiarism is eliminated and not considered for publication.

Authors should cite publications that have been influential in the nature of the Article submitted to arbitration.

Information services

Indexation - Bases and Repositories

RESEARCH GATE (Germany)
GOOGLE SCHOLAR (Citation indices-Google)
REDIB (Ibero-American Network of Innovation and Scientific Knowledge- CSIC)
MENDELEY (Bibliographic References Manager)
DULCINEA (Spanish scientific journals)
UNIVERSIA (University Library-Madrid)
SHERPA (University of Nottingham - England)

Publishing Services

Citation and Index Identification H
Management of Originality Format and Authorization
Testing Article with PLAGSCAN
Article Evaluation
Certificate of Double-Blind Review
Article Edition
Web layout
Indexing and Repository
ArticleTranslation
Article Publication
Certificate of Article
Service Billing

Editorial Policy and Management

21 Santa Lucía, CP-5220. Libertadores -Sucre – Bolivia. Phones: +52 1 55 6159 2296, +52 1 55 1260 0355, +52 1 55 6034 9181; Email: contact@ecorfan.org www.ecorfan.org

Journal Simulation and Laboratory

2410 3462
ISSN 2410 - 3462